R-13-33

Slow strain rate tensile testing of friction stir welded Cu-OFP

Constitutive equations for creep

Rolf Sandström, Sakander Waqas Ahmad,
Kirti Teja Pasupuleti, Meysam Mahdavi Shahri
Department of Materials Science and Engineering, KTH

August 2017

Svensk Kärnbränslehantering AB
Swedish Nuclear Fuel
and Waste Management Co

Box 3091, SE-169 03 Solna
Phone +46 8 459 84 00

ISSN 1402-3091
SKB R-13-33
ID 1400799

August 2017

Slow strain rate tensile testing of friction stir welded Cu-OFP

Constitutive equations for creep

Rolf Sandström, Sakander Waqas Ahmad,
Kirti Teja Pasupuleti, Meysam Mahdavi Shahri
Department of Materials Science and Engineering, KTH

Keywords: Copper, Creep, Weldment, Tensile testing, Constitutive equations.

Abstract

Copper canisters intended for disposal of spent nuclear fuel will be exposed to external pressure in the repository. This gives rise to creep deformation in the copper. It is likely that the increase in pressure will be quite gradual. The ideal tool to simulate this type of loading is slow strain rate tensile tests (SSRT). SSRT tests have previously been performed for base material of phosphorus alloyed oxygen free copper Cu-OFP. In the present paper SSRT is performed for friction stir welded Cu-OFP. The weld zone, the heat affected zone (HAZ) and cross weld specimens have been studied. The different weld microstructures have slightly higher yield strength and lower work hardening rate than the base metal. Basic constitutive equations are formulated for the different weld zones. Both strain controlled and load controlled situations are covered. Numerical examples of applications of the constitutive equations are given to simplify the use of them.

Contents

1	**Introduction**	7
2	**Material and specimens**	9
3	**Testing**	13
4	**Model**	15
4.1	Basic model	15
4.2	Stress strain curves	17
4.3	Primary and secondary creep	18
4.4	Numerical solution of the creep equation	19
4.5	Multiaxial creep	20
4.6	Parameter values in the models	21
5	**Results from slow strain rate tensile tests**	23
6	**Model results for stress strain curves**	29
7	**Creep strain versus time curves**	35
8	**Discussion**	39
9	**Conclusions**	41
10	**Acknowledgements**	43
References		45
Appendix A		47

1 Introduction

In Sweden, spent nuclear fuel is planned to be placed in waste packages with an external cylindrical copper canister according to the KBS-3 concept (Raiko et al. 2010, Rosborg and Werme 2008). The canisters will gradually be exposed to an external pressure of about 15 MPa due to the hydrostatic pressure from a 500 m water pillar and the swelling pressure from the surrounding bentonite clay (Raiko et al. 2010). Due to this pressure, creep deformation will take place in the canisters. Experimentally, creep deformation has primarily been studied with the help of creep strain versus time tests. A survey of this work is available (Andersson-Östling and Sandström 2009). In most of the creep modelling it has been assumed that the full load is applied directly (Jin and Sandström 2008, 2009a, b). This is natural since the creep data are practically always generated with a constant applied load, although ramping of the loading has also been studied (Andersson-Östling and Sandström 2011, Jin and Sandström 2013).

In the repository, however, the increase in mechanical loading can be expected to be slow and gradual. To simulate this situation it is natural to use slow strain rate tensile (SSRT) tests. This technique has also been used to successfully develop fundamental models for primary creep (Sandström 2012). SSRT tests have been performed for Cu-OFP (pure oxygen free copper alloyed with about 50 ppm P). Yao studied cold deformed material (Yao and Sandström 2000) and Sandström and Hallgren as hot worked Cu-OFP (Sandström and Hallgren 2012). These investigations cover the temperature interval 20 to 175 °C and strain rates from 1×10^{-7} to 0.1 1/s. In Sandström and Hallgren (2012) both tension and compression were studied.

Slow strain rate tests for welds have not been carried out before. The purpose of the present report is to perform slow strain rate tensile tests for friction stir welded copper and use the results to develop basic models for strain and stress controlled deformation in welds. Weld zone, heat affected zone, and cross weld conditions are covered. The temperature range chosen is 20 to 175 °C, i.e. the same as for the parent metal. The three strain rates tested are 1×10^{-7}, 3×10^{-6}, and 1×10^{-4} 1/s.

For making predictions of creep deformation over the extensive periods that the copper canisters have to stay intact in the repository, the use of fundamental models is vital. This can be understood from the following argument. Let us consider extrapolation of creep data for Cu-OFP at 75 °C as an example. This is well within the range of temperatures that the canister will be exposed to in the repository. At this temperature creep test results are available for up to 15 000 h, i.e. about 1.5 years. It is well established that the best experts on creep extrapolation can safely make an extrapolation of a factor of three in time but only occasionally by a factor of 10 (Holdsworth et al. 2008). At 75 °C, creep data are mainly available in the stress range 160 to 180 MPa. An extrapolation in time by a factor of three or ten means that we can make predictions for effective stresses down 155 and 150 MPa, respectively. That this is very far from adequate is directly evident by considering that the effective stress level in the canister tube shell is about 125 MPa in typical loading cases, and where creep is taken place (Jin and Sandström 2013). Let us on the other hand consider a fundamental creep model that has been developed (Sandström 2012). It has been experimentally verified that this model is approximately valid down to effective stresses of 40 MPa.

In this report fundamental models for the creep behaviour of weld zones are formulated. They are developed in such a way that they should be valid down to stresses much lower than the experimental stress range 150 to 180 MPa in creep tests.

2 Material and specimens

The test materials were taken from two friction stir welded copper canister rings referred to as a and b. For ring a the tube had the designation T27-R10, the lid TX219, and weld FSWL75 For ring b the tube had the designation T66-R3, the lid TX230, and the weld FSWL84. The composition of the parent metal is given in Table 2-1. The values were measured in the ingots before hot working. The welding of FSWL75 was performed in air, whereas FSWL84 was carried out with argon as shielding gas.

Table 2-1.Composition of parent metal in the canister tube and lid (wt. ppm).

Element	Top tube, ring a	Bottom tube, ring a	Lid, ring a	Tube, ring b	Lid, ring b
Cu (%)	99.992	99.993		99.991	
Ag	13.9	13.6	10	11	12
As	0.98	1.05	< 0.5	0.29	< 1
Bi	0.21	0.21	< 0.5	0.13	< 1
Cd	< 0.003	< 0.003	< 0.1	< 0.003	< 1
Co	< 0.006	< 0.006	< 0.4		< 1
Cr	0.19	0.20	< 1		< 1
Fe	1.2	1.0	1	0.25–0.36	< 1
H	0.24	0.37		0.28–0.31	
Hg				< 0.5	
Mn	0.00	0.00	< 0.5	< 0.1	< 0.5
Ni	0.3	0.3	< 1	< 0.2	2
O	1.0	2.5	1–2	1.5–1.7	1–2
P	60	50	59	62–63	46–60
Pb	0.22	0.30	1	0.2	< 1
S	5.8	5.9	5	4.0–4.1	6
Sb	0.49	0.59	0.5	0.06	1
Se	0.46	0.52	< 1	0.2	< 1
Si	< 0.2	< 0.2			
Sn	0.051	0.081	< 0.2	0.03	< 0.5
Te	0.24	0.24	1.0	0.11–0.12	< 1
Zn	0.00	0.00	< 1	< 0.1	< 1

The element that gives the main influence on the creep properties is the phosphorus content. It is in its optimal range 50–70 ppm (Andersson et al. 1999). No other element is likely to have a significant effect.

In order to prepare the specimens from the cylindrical lid including the weld, water cutting was used. Slices of 4 degrees were cut out for cross weld specimens and 23 degree slices for weld, HAZ and base material specimens, see Figure 2-1. Figure 2-2 shows how the slices were cut. In total 12 slices from ring a and 8 slices from ring b were prepared for the tensile specimens.

The surface of the slices were etched in order to locate the weld and heat affected zone area, Figure 2-3. It was observed that weld centre line is 63 mm away from left side in Figure 2-4. For each slice two specimens were taken from the upper and lower part of the weld in Figure 2-4a. Also two specimen were taken from HAZ (on the left and right side of the weld nugget in Figure 2-4) at a distance of 44 mm apart. Cross weld specimens were also prepared from the thin sections, see Figure 2-4. In this case the weld was not exactly at the centre of the specimen.

Tensile specimen were made with gauge length of 50 mm and total length of 130 mm, see Figure 2-5. However, the knife edges were not produced in this series of testing. These pieces were machined to the tensile specimens using a CNC machine.

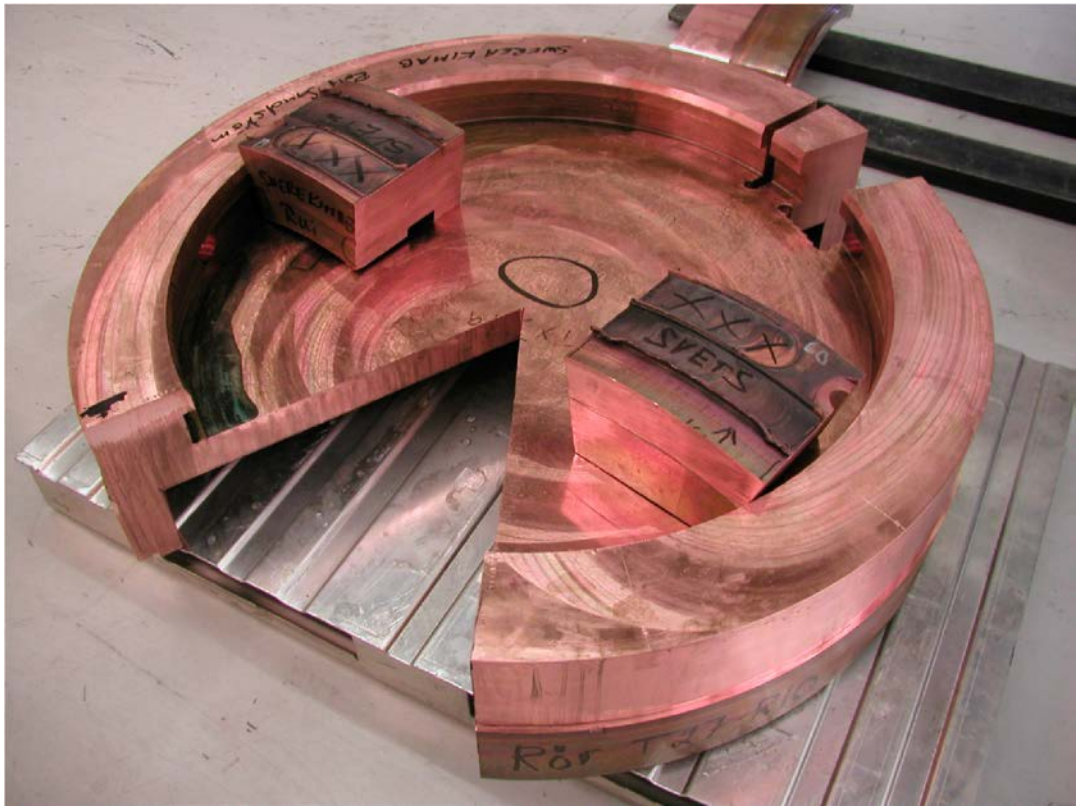

Figure 2-1. *Welded lid and ring from which specimens were extracted.*

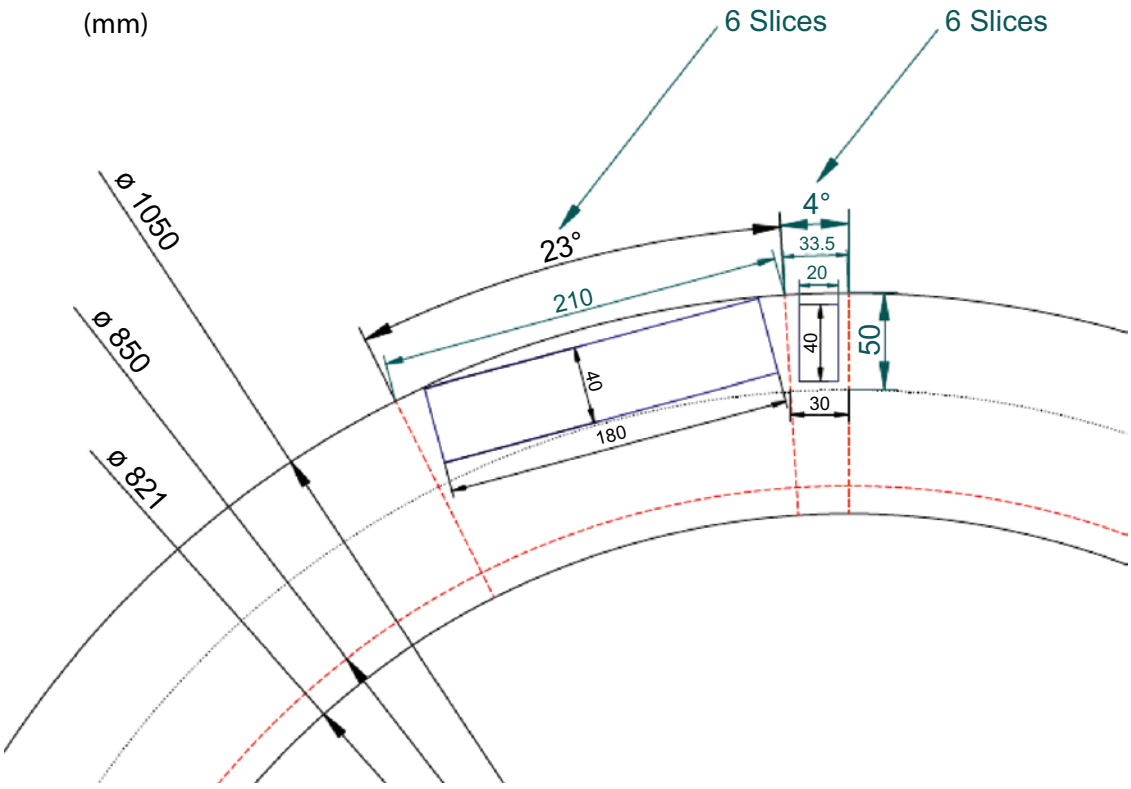

Figure 2-2. *Twelve slices were cut from the ring.*

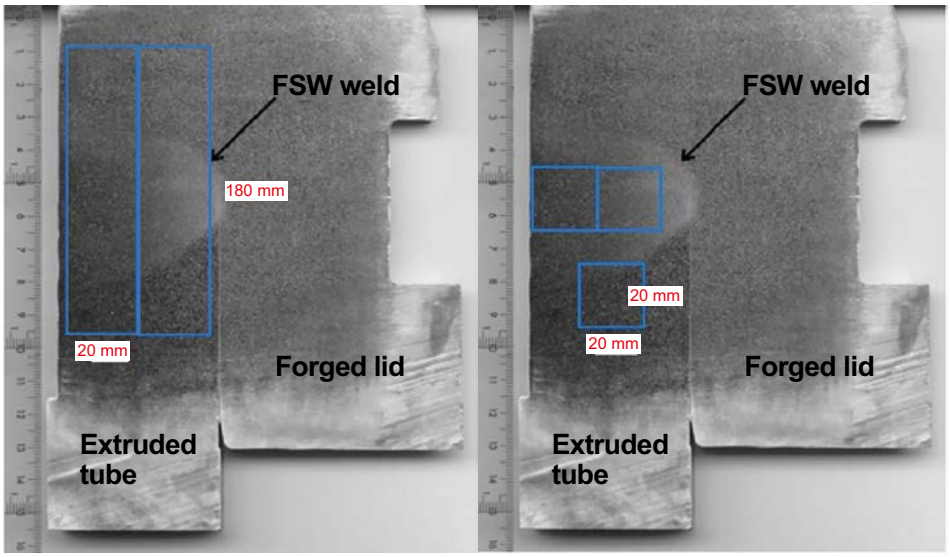

Figure 2-3. *Etched slices on the surface. The left hand figure shows the position for cross weld samples and the right hand figure the position of weld and HAZ samples.*

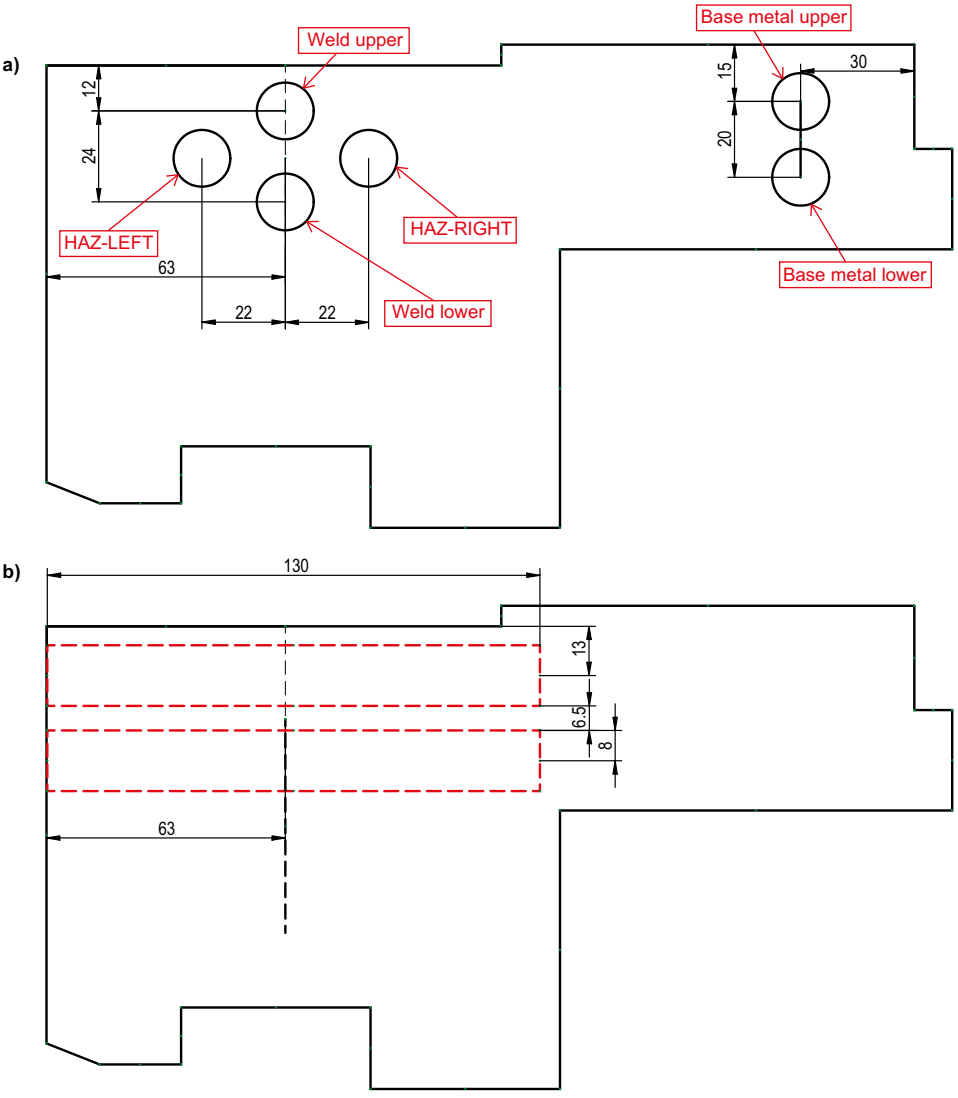

Figure 2-4. *Location of extracted specimens; a) base metal, weld metal and HAZ; b) cross weld specimens (dimensions are in mm).*

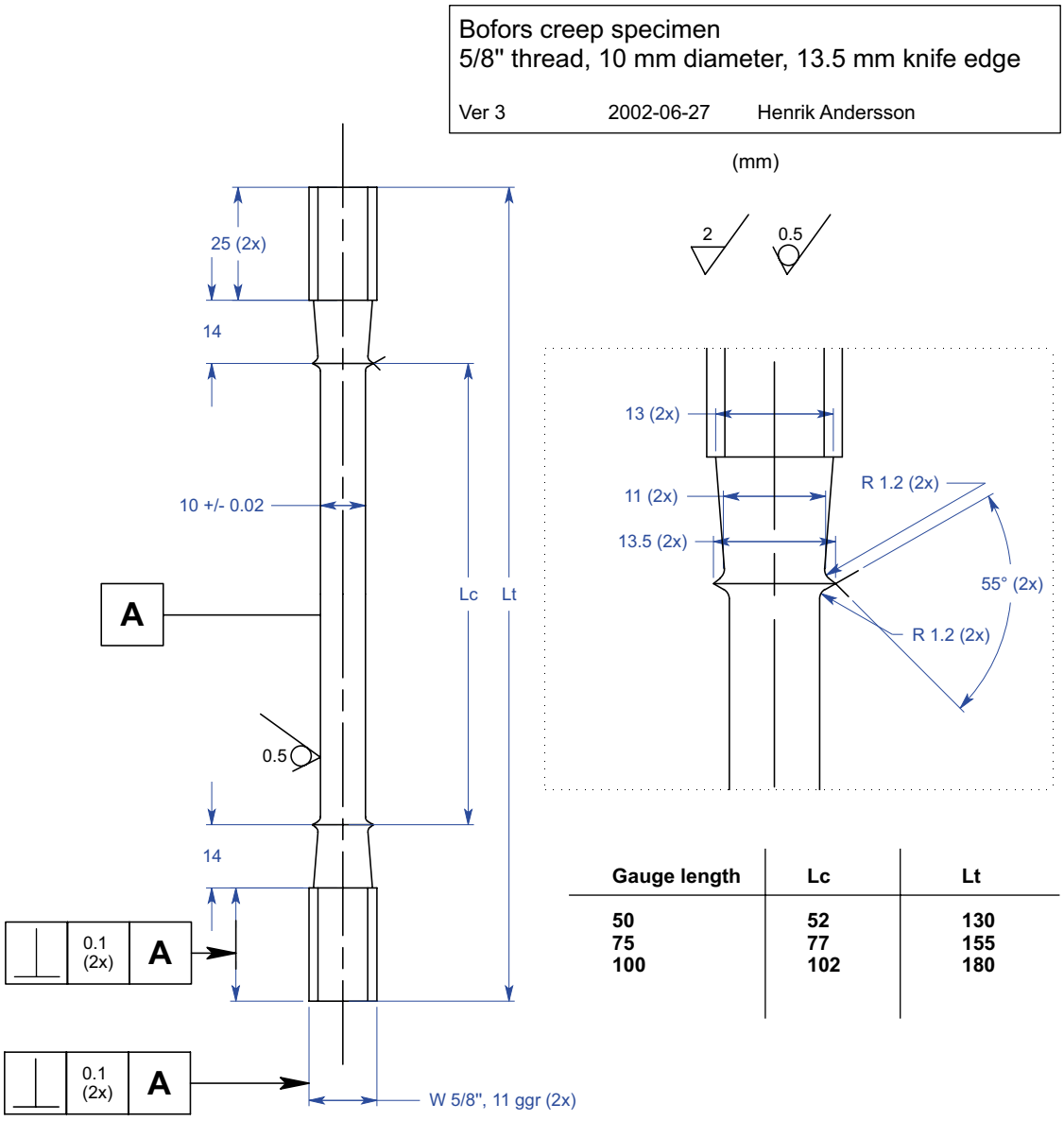

Gauge length	Lc	Lt
50	52	130
75	77	155
100	102	180

Figure 2-5. *Tensile specimen.*

3 Testing

The mechanical testing was conducted using two uniaxial tensile testing machines Swetest NT 2005, which are electromechanical machines. In the testing of specimens from ring a, an extensometer of type Epsilon (model 3542-050M-HT2) was used to record the specimen elongation. The extensometer has a maximum elongation limit of 2.5 mm (5 % strain). When the strain exceeded the limit 5 %, the extensometer was removed, zeroed and put back again. This procedure involves small discontinuities in the data which were corrected for later on. For ring b a new extensometer with 20 mm maximum displacement of the same brand was used.

Tests were conducted using the encoder control channel on the tensile machine. Machine parameters were optimised for the specific test conditions and material used. These parameters include the PID values and filters on the load and extensometer reading. The filters reduce the noise contribution from the load and extensometer signals. The sample is loaded using machine software by specifying the velocity to the machine. The load is measured in kN in the load cell. The encoder movement and the extensometer give extension in mm for the sample. The test arrangement also includes a furnace to maintain the required temperature of the specimen.

The testing programme is shown in Table 3-1. A total of 40 specimens were successfully tested at 32 different strain rates and temperatures. Eight conditions were tested both for ring a and ring b.

Table 3-1. Test conditions.

Strain rate, 1/s	20 °C	75 °C	125 °C	175 °C	Max Strain
1×10^{-4}	CW	CW	CW	CW	Rupture
	WM	WM	WM	WM	
	HAZ	HAZ	HAZ	HAZ	
3×10^{-6}	CW	CW	CW	CW	20 %
	WM	WM	WM	WM	
	HAZ	HAZ	HAZ		
1×10^{-7}	CW	CW	CW	CW	5 %
	WM	WM	WM		
	HAZ	HAZ			

CW, cross weld specimens; WM, weld zone; HAZ, heat affected zone.

The used strain rates were 1×10^{-4}, 3×10^{-6}, and 1×10^{-7} 1/s at temperatures 20, 75, 125 and 175 °C. The tests conducted at a strain rate 1×10^{-4} 1/s were strained till rupture, tests at a strain rate 3×10^{-6} till 20 % elongation and the tests with a strain rate of 1×10^{-7} till 5 % elongation of the gauge length of the specimen. The tests took 3 h, 1.5 days and 9 days for a strain rate of 1×10^{-4}, 3×10^{-6}, and 1×10^{-7} 1/s, respectively. Before starting the test, the initial dimensions were noted to facilitate the subsequent studies. The samples were mounted in the machine using the holding fixtures to ensure that the uniaxial tensile testing took place under controlled conditions. The Epsilon extensometers were attached to specimen very precisely to measure the strain in term of the extension. The specimens were heated for one hour before the start of the test to homogenise the temperature distribution. For each sample, data for force (load), stroke travel, extensometer extension, time, and temperature were collected. Extensometer extension and load data were used to determine the stress-strain curves. The yield strength values were assessed at 0.2 % strain offset.

4 Model

4.1 Basic model

In Sections 4.1 to 4.3, the background to models for parent metal that have previously been published are summarised (Sandström and Hallgren 2012, Sandström 2012). During plastic deformation three main processes take place. Work hardening raises the strength by generation of new dislocations and thereby increases their density. The increase of the dislocation density raises the energy content of the material. There is a driving force to reduce the energy content. The mechanism that makes this possible is called recovery. During recovery dislocations of opposite sign combine and annihilate each other, which reduces the density of dislocations. There are two types of recovery. One is static recovery that is time dependent. The other is dynamic recovery that is strain dependent.

The work hardening of polycrystalline materials can be described with the help of the Orowan equation for the dislocation density ρ

$$\frac{d\rho}{d\varepsilon} = \frac{m}{bL} \qquad \text{(work hardening)} \qquad \text{Eq (4-1)}$$

ε is the strain, m the Taylor factor, b Burger's vector and L the "spurt" distance which the dislocation moves in each elementary release during deformation. L can be related to the barriers in the materials such as grains or subboundaries. The most common assumption is that L is controlled by the forest of dislocations, i.e. it is related to the average distance between the dislocations $1/\rho^{1/2}$.

$$L = \frac{c_L}{\rho^{1/2}} \qquad \text{Eq (4-2)}$$

c_L is a constant that is much larger than unity. How to find the size of c_L will be discussed below. The contribution from dynamic recovery can be expressed as (Bergström 1972, Roberts and Bergström 1973)

$$\frac{d\rho}{d\varepsilon} = -\omega\rho \qquad \text{(dynamic recovery)} \qquad \text{Eq (4-3)}$$

Roters et al. (2000) gave a basic derivation of Eq (4-3) and at the same time provided a value for the constant ω

$$\omega = \frac{m}{b} d_{\text{int}} \left(2 - \frac{1}{n_{\text{slip}}}\right) \qquad \text{Eq (4-4)}$$

d_{int} is the interaction distance between dislocations (= 2.5 b) and n_{slip} the number of independent slip systems (= 12 for fcc metals) (Sandström 2012). It will be seen below that the interaction distance is 2 b for the weld zones. Static recovery takes into account how climbing (and gliding, see below) dislocations of opposite sign moves towards each other and finally annihilate each other (Friedel 1964)

$$\frac{d\rho}{dt} = -2\tau_{\text{L}} M \rho^2 \qquad \text{(static recovery)} \qquad \text{Eq (4-5)}$$

t is the time, τ_{L} the dislocation line tension, and M the dislocation mobility. Notice that we have strain derivatives in Eq (4-1) and Eq (4-3) but a time derivative in Eq (4-5). The climb mobility of dislocations was first derived by Hirth and Lothe (Hirth and Lothe 1968)

$$M_{\text{climb}} = \frac{D_{\text{s0}} b}{k_{\text{B}} T} e^{\frac{\sigma b^3}{k_{\text{B}} T}} e^{-\frac{Q}{RT}} \qquad \text{Eq (4-6)}$$

where T is the absolute temperature, σ the applied stress, D_{s0} the preexponential coefficient for self-diffusion, Q the activation energy for self-diffusion, k_{B} Boltzmann's constant, and R the gas constant.

To describe how the dislocation density ρ develops during plastic deformation, the contributions from work hardening Eq (4-1), dynamic recovery Eq (4-3), and static recovery Eq (4-5) are added.

$$\frac{d\rho}{d\varepsilon} = \frac{m}{bL} - \omega\rho - 2\tau_L M\rho^2 / \dot{\varepsilon} \qquad \text{Eq (4-7)}$$

To change the time derivative to a strain derivative, the static recovery term is divided by the strain rate ε̇. When representing static recovery not only climb of dislocation but also glide must be taken into account. This is possible by forming an integrated expression for glide and climb. This was done in Sandström and Andersson (2008a) using an expression from Kocks et al. (1975). The resulting expression for the combined mobility for climb and glide for Cu-OF is

$$M_{OF}(T,\sigma) = \frac{D_{s0}b}{k_B T} e^{\frac{\sigma b^3}{k_B T}} e^{-\frac{Q}{RT}\left[1-\left(\frac{\sigma}{\sigma_{imax}}\right)^2\right]} \qquad \text{Eq (4-8)}$$

σ_{imax} is the tensile strength at room temperature. The dislocation mobility for phosphorus alloyed copper, Cu-OFP can be expressed as (Sandström 2016a, b)

$$M(T,\sigma) = M_{OF}(\sigma - \sigma_{break}, T) f_Q \qquad \text{Eq (4-9)}$$

f_Q is a factor describing the influence of phosphorus as a solid solution hardener (Korzhavyi and Sandström 2015, Sandström and Andersson 2008b). It is given by

$$f_Q = e^{-U_P^{max}/RT}$$

The maximum interaction energy between a P solute and a dislocation is (Korzhavyi and Sandström 2015, Sandström and Andersson 2008b)

$$U_P^{max} = \frac{1}{\pi}\frac{(1+\nu)}{(1-\nu)} G\Omega_0 \varepsilon_P \frac{b}{r_{core}} \qquad \text{Eq (4-10)}$$

ν is Poisson's ratio, Ω_0 the atomic volume, ε_P the linear misfit for P atoms, and r_{core} the dislocation core radius. The value of the interaction energy is 8 220 J/mol. The phosphorus atoms form Cottrell atmospheres around the dislocations. The dislocations must break away from their phosphorus atmospheres in order to move.

The stress σ_{break} is required for the dislocations to break away from the Cottrell atmospheres of P atoms (Sandström and Andersson 2008b). σ_{break} is given by the following expression

$$\sigma_{break} = \frac{U_P^{max}}{b^3}\int_{y_L}^{y_R} c_P^{dyn}\, dy \qquad \text{Eq (4-11)}$$

The integration is performed around a dislocation (± 20 *b*).

Equation (4-7) is now a general equation for the development of the dislocation density during plastic deformation in copper. As will be illustrated, it can be used to describe stress strain curves from constant strain rate tests as well as creep strain versus time curves from creep tests at constant load. All parameters can be found from how the different contributions were derived, see Table 4-1. None is used for adjustment to the mechanical test results.

4.2 Stress strain curves

In stress strain tests at constant strain rates, the last term in Eq (4-7), the static recovery term, can usually be neglected. This can be verified by direct computation of the static recovery contribution. With this simplification, Eq (4-7) takes the form

$$\frac{d\rho}{d\varepsilon} = \frac{m}{bL} - \omega\rho \qquad \text{Eq (4-12)}$$

The dislocations give rise to a stress that is given by Taylor's equation

$$\sigma = \sigma_y + m\alpha Gb\sqrt{\rho} \qquad \text{Eq (4-13)}$$

where α is a constant and G is the shear modulus. Inserting Eq (4-13) and using Eq (4-2) gives

$$\frac{d\sigma}{d\varepsilon} = \frac{\omega}{2}(K + \sigma_y - \sigma) \qquad \text{Eq (4-14)}$$

where

$$K = \frac{m^2\alpha G}{c_L\omega} \qquad \text{Eq (4-15)}$$

Equation (4-14) can be integrated directly. Taking into account that the stress is equal to the yield strength σ_y at zero strain (neglecting the elastic contribution which is unimportant in this context) gives

$$\sigma = \sigma_y(T,\dot{\varepsilon}) + (\sigma_{max} - \sigma_y(T,\dot{\varepsilon}))(1 - e^{-\omega\varepsilon/2}) \qquad \text{Eq (4-16)}$$

where $\sigma_{max} = K + \sigma_y$ is the maximum stress in the flow curve. Eq (4-16) is usually referred to as the Kocks-Mecking equation (Mecking and Kocks 1981). However, it was first presented in Bergström (1972). Eq (4-16) will be used in Chapter 6 together with experimental stress strain curves.

To find the value of the constant c_L the assumption is made that the maximum value of the two last terms in Eq (4-7) are the same, which has been experimentally verified in Sandström and Hallgren (2012). The dynamic recovery controls the maximum stress during strain controlled deformation at a given strain rate and the static recovery the stationary creep rate at a given stress. Assuming that these two types of tests are controlled by the same deformation mechanism, which is a natural assumption, the results should be related to each other in such a way that the results from one test could be transferred to the other test. This requires that the maximum value of the two last terms in Eq (4-7) are the same. The maximum value of the dislocation density is obtained from Eq (4-12) and using Eq (4-2)

$$\rho_{max} = \left(\frac{m}{bc_L\omega}\right)^2 \qquad \text{Eq (4-17)}$$

With this value for the dislocation density in the two last terms in Eq (4-7) gives

$$\omega = 2\tau_L M(T,\sigma_\rho)\rho_{max}/\dot{\varepsilon} \qquad \text{Eq (4-18)}$$

where σ_ρ is obtained from the Taylor Eq (4-13). To find the c_L value, Eq (4-18) together with Eq (4-13) and Eq (4-17) are solved by iteration.

In Eq (4-16) the yield strength depends on the temperature and the strain rate. A model for this dependence is derived in Sandström and Hallgren (2012).

$$\sigma_y(T,\dot{\varepsilon}) = \sigma_y(T_0,\dot{\varepsilon}_0)\frac{G(T)}{G(T_0)}\left(\frac{\dot{\varepsilon}}{\dot{\varepsilon}_0}\right)^{(1/n_N)} \qquad \text{Eq (4-19)}$$

Equation (4-19) is somewhat simplified in comparison to the expression in Sandström and Hallgren (2012), since the climb dependent part has been removed. Eq (4-19) has been fully verified for parent metal by comparison to the experimental data in Sandström and Hallgren (2012). The validity is also demonstrated in Chapter 6 for material in the different weld zones (Figure 6-1 and Figure 6-2). The value of the yield strength is related to a reference condition $\dot{\varepsilon} = \dot{\varepsilon}_0 = 1 \times 10^{-4}$ 1/s and $T = T_0 = 20$ °C for Cu-OFP. The strain rate dependence is formulated with the help of the creep exponent n_N. This exponent can be determined from the creep rate in Eq (4-21) below. Examples of n_N values are 111, 86, 66, and 49 at 20, 75, 125 and 175 °C for $\dot{\varepsilon} = \dot{\varepsilon}_0 = 1 \times 10^{-4}$ 1/s for Cu-OFP.

4.3 Primary and secondary creep

During secondary creep, the strain rate is approximately constant and the creep is said to be stationary. During this stage the strain and time derivatives of the dislocation density become zero. From Eq (4-7) we then find that

$$\dot{\varepsilon} = \frac{2bc_L\tau_L}{m} M\rho^{3/2}/(1-\frac{bc_L\omega}{m}\rho^{1/2}) \qquad \text{Eq (4-20)}$$

Equation (4-20) is combined with Eq (4-13) when it is applied in creep. Two assumptions are commonly made. i) The last term in the brackets in Eq (4-20), the dynamic recovery term, is neglected. ii) The second assumption is that the yield strength in Eq (4-13) is disregarded. It is typically much smaller than the applied stress for copper in particular at low strain rates and higher temperatures. With these assumptions the stationary creep rate takes the following form

$$\dot{\varepsilon}_{stat} = \frac{2bc_L\tau_L}{m}\left(\frac{\sigma-\sigma_{break}}{\alpha mGb}\right)^3 M_{OF}(\sigma-\sigma_{break},T) f_Q = h(\sigma,T) \qquad \text{Eq (4-21)}$$

Further details of the derivation can be found in Sandström and Andersson (2008a, b). Eq (4-21) is a result of the balance between work hardening and static recovery. However, the numerator in Eq (4-20) can give a significant contribution to tertiary creep. This has been demonstrated for cold worked materials (Sandström 2016c).

Equation (4-21) covers tests at constant load and Eq (4-16) tests at constant strain rate. To derive an expression for strain time curves during primary creep, the two equations are combined. Above it was shown that it is the maximum stress derived from Eq (4-5) that approximately corresponds to the creep stress in the equation for the stationary creep rate. This maximum stress is the same as the maximum stress in the flow curves with the assumptions made. The stress that is introduced in Eq (4-21) is consequently σ_{max}. Further details of this derivation can be found in Sandström (2012)

$$\frac{d\varepsilon}{dt} = h(\sigma_y(T,\dot{\varepsilon}) + \frac{\sigma-\sigma_y(T,\dot{\varepsilon})}{1-e^{-\omega\varepsilon/2}}, T) \qquad \text{Eq (4-22)}$$

In Eq (4-22), σ is the applied stress in the creep test. An abbreviated version of Eq (4-21) in the form of $h(\sigma,T)$ is used. The temperature and strain rate dependence of the yield strength is now explicitly given. Eq (4-22) is a differential equation for the creep strain. It can be integrated to derive creep strain curves covering primary and secondary creep. That secondary creep can be handled is evident by inserting a large strain making $\omega\varepsilon$ much larger than unity. The denominator then takes the value unity and Eq (4-21) is recovered. During primary creep the strain is small. This makes the stress expression in Eq (4-22) quite large. In this way the large strain rates during primary creep can be described.

An alternative approach for finding an equation for primary creep is given in Sandström (2016c). According to this approach the dislocations generated during creep create a back stress that gradually reduces the strain rate during primary creep.

4.4 Numerical solution of the creep equation

There are different ways of integrating Eq (4-2) numerically. The complication is that the yield strength according to Eq (4-19) depends on the strain rate. The most direct way of solving Eq (4-22) is by iteration. The strain rate from Eq (4-22) is inserted in Eq (4-19) and then the process is repeated until the strain rate from Eq (4-22) is not changed anymore. In this way the total stress in Eq (4-22) and strain rate is found for each time step. Thus, an iteration has to be performed in each time step. This way of solving Eq (4-22) is referred to as *stress adaptation*.

It is possible to simplify the integration of Eq (4-22). We assume that the function $h(\sigma,T)$ can be represented by a Norton equation

$$\frac{d\varepsilon}{dt} = h(\sigma,T) = A_{\mathrm{N}}(T)\sigma^{n_{\mathrm{N}}} \qquad \text{Eq (4-23)}$$

Inserting this expression and the equation for the yield strength Eq (4-19) into Eq (4-22) and making some simple transformations give

$$\left(\frac{\dot{\varepsilon}}{A_{\mathrm{N}}}\right)^{1/n_{\mathrm{N}}} = \sigma_{\mathrm{y}}(T,\dot{\varepsilon}_0)\frac{G(T)}{G(T_0)}\left(\frac{\dot{\varepsilon}}{\dot{\varepsilon}_0}\right)^{(1/n_{\mathrm{N}})} + \frac{\sigma-\sigma_{\mathrm{y}}(T,\dot{\varepsilon}_0)\frac{G(T)}{G(T_0)}\left(\frac{\dot{\varepsilon}}{\dot{\varepsilon}_0}\right)^{(1/n_{\mathrm{N}})}}{1-e^{-\omega\varepsilon/2}} \qquad \text{Eq (4-24)}$$

We introduce the abbreviations

$$a_{\mathrm{N}} = A_{\mathrm{N}}{}^{1/n_{\mathrm{N}}} \qquad b_{\mathrm{N}} = \sigma_{\mathrm{y}}(T,\dot{\varepsilon}_0)\frac{G(T)}{G(T_0)}/\dot{\varepsilon}_0{}^{1/n_{\mathrm{N}}} \qquad \text{Eq (4-25)}$$

Inserting the abbreviations Eq (4-25) into Eq (4-24) and solving for $\dot{\varepsilon}$ gives

$$\dot{\varepsilon}^{1/n_{\mathrm{N}}} = \frac{1}{1/a - b + \frac{b}{1-e^{-\omega\varepsilon/2}}}\,\frac{\sigma}{1-e^{-\omega\varepsilon/2}} \qquad \text{Eq (4-26)}$$

From this expression we can directly get the yield strength

$$\sigma_{\mathrm{y}}(T,\dot{\varepsilon}) = \sigma_{\mathrm{y}}(T,\dot{\varepsilon}_0)\frac{G(T)}{G(T_0)}\left(\frac{\dot{\varepsilon}}{\dot{\varepsilon}_0}\right)^{1/n_{\mathrm{N}}} = b\dot{\varepsilon}^{1/n_{\mathrm{N}}} = \frac{\sigma}{\left(\frac{1}{ab}-1\right)\left(1-e^{-\omega\varepsilon/2}\right)+1} \qquad \text{Eq (4-27)}$$

We have now an expression for the yield strength that depends on the strain ε but not on the strain rate. If this expression is inserted into equation Eq (4-22), it can be integrated directly without the need for iteration in each time step. This method is referred to as *expansion integration.* One more thing to emphasize is that the Norton equation should be determined for the total stress σ_{tot} in Eq (4-22), i.e. the stress expression in the function $h(\sigma,T)$.

$$\sigma_{\mathrm{tot}} = \sigma_{\mathrm{y}}(T,\dot{\varepsilon}) + \frac{\sigma-\sigma_{\mathrm{y}}(T,\dot{\varepsilon})}{1-e^{-\omega\varepsilon/2}} \qquad \text{Eq (4-28)}$$

Another way of numerically solving Eq (4-22) will also be described. We start by rewriting Eq (4-16) in the following way by extracting the strain rate dependence, assuming that σ_{y} and K have the same strain rate dependence, which is approximately the case

$$\sigma = \left[\sigma_{\mathrm{y}}(T) + K(T)\left(1-\mathrm{e}^{-\omega\varepsilon/2}\right)\right]\left(\frac{\dot{\varepsilon}}{\dot{\varepsilon}_{\mathrm{k}}}\right)^{1/n_{\mathrm{N}}} \qquad \text{Eq (4-29)}$$

The reference is not known for the strain rate $\dot{\varepsilon}_0$ but for a rate corresponding to the maximum stress

$$\dot{\varepsilon}_k = A_N(\sigma_y(T) + K(T))^{n_N} \quad \text{Eq (4-30)}$$

A_N and n_N are determined from the total stress σ_{tot} in Eq (4-16) in the same way as in the previous procedure

$$A_N \sigma_{tot}^{n_N} = h(\sigma_{tot}, T) \quad \text{Eq (4-31)}$$

Next, Eq (4-29) is rewritten in the following form

$$\frac{\dot{\varepsilon}}{\dot{\varepsilon}_k} = \left\{ \frac{\sigma}{\sigma_y(T) + K(T)(1 - e^{-\omega\varepsilon/2})} \right\}^{n_N} \quad \text{Eq (4-32)}$$

Combining Eq (4-30) and Eq (4-32) gives

$$\dot{\varepsilon} = A_N \left\{ \frac{\sigma(\sigma_y(T) + K(T))}{\sigma_y(T) + K(T)(1 - e^{-\omega\varepsilon/2})} \right\}^{n_N} \quad \text{Eq (4-33)}$$

This Norton equation can be transformed back in the form of Eq (4-22)

$$\dot{\varepsilon} = h\left(\frac{\sigma(\sigma_y(T) + K(T))}{\sigma_y(T) + K(T)(1 - e^{-\omega\varepsilon/2})}, T \right) \quad \text{Eq (4-34)}$$

The selection of the strain rate at which $\sigma_y(T)$ and $K(T)$ are determined is not critical since they have about the same strain rate dependence. It is practical to use the stationary creep rate from Eq (4-22). Eq (4-34) can be integrated directly without iterations. In comparison to the previous numerical approach, it has the advantage that it is not singular at small strains. This method is referred to as *max stress integration*.

4.5 Multiaxial creep

The purpose of the present report is to derive constitutive equations that can be applied to components, such as the copper canister. In such cases multiaxial stresses are of importance. Using Odqvist's equation (Odqvist 1966), Eq (4-22) can be transferred to multiaxial stress states

$$\frac{d\boldsymbol{\varepsilon}}{dt} = \frac{3}{2} \frac{d\varepsilon^{eff}}{dt} \frac{\boldsymbol{\sigma}'}{\sigma_{eff}} \quad \text{Eq (4-35)}$$

where $\boldsymbol{\varepsilon}$ is the creep strain tensor, σ_{eff} the effective (von Mises) stress and $\boldsymbol{\sigma}$' the stress deviator tensor. The effective creep strain rate is given by

$$\frac{d\varepsilon^{eff}}{dt} = h\left(\sigma_y(\dot{\varepsilon}^{eff}) + \frac{\sigma_{eff} - \sigma_y(\dot{\varepsilon}^{eff})}{1 - e^{-\omega\varepsilon^{eff}/2}}, T\right) \quad \text{Eq (4-36)}$$

Equation (4-36) has successfully been applied to model creep in notched tensile specimens (Wu et al. 2010, Sandström et al. 2009).

4.6 Parameter values in the models

The parameter values used in the computations are listed in Table 4-1. The yield strengths at the reference condition for the various microstructures are given in Table 6-1.

Table 4-1. Values of constants used in computations.

Parameter description	Parameter	Value	Reference
Coefficient for self-diffusion	D_{s0}	1.31×10^{-5} m^2/s	(Neumann et al. 1999)
Activation energy for self-diffusion	Q_{eff}	198 000 J/mol	(Neumann et al. 1999)
Burgers' vector	b	2.56×10^{-10} m	
Taylor factor	m	3.06	
Poisson's ratio	v	0.308	(ASM 1991)
Constant	α	$(1-\nu/2)/2\pi(1-\nu) = 0.19$	(Orlová 1991, Horiuchi and Otsuka 1973)
Max back stress	σ_{imax}	257 MPa	(Sandström and Andersson 2008a)
Dislocation line tension	τ_L	$Gb^2/2 = 7.94 \times 10^{-16}$ MN at room temperature	(Dieter 1986)
Boltzmann's constant	k_B	1.381×10^{-23} J/grad	
Gas constant	R	8.31 J/(mol · K)	
Shear modulus	G	45 400 $(1-7.1 \times 10^{-4}\ (T-20))$, MPa, T in °C	(Ledbetter and Naimon 1974)
Atomic volume	Ω_0	$b^3/\sqrt{2} = 1.18 \times 10^{-29}$ m^3	
Lattice misfit for P atom	ε_P	0.055	(Sandström and Andersson 2008a, b)
Dynamic recovery constant	ω	14.67 for parent metal 11.73 for weld zones	(Sandström and Hallgren 2012), This work
Dislocation core radius	r_{core}	$1.3b = 7.68 \times 10^{-10}$ m	(Wang et al. 2011)
P content for the prediction of stress strain curves	x_P	123 at. ppm (60 wt. ppm) parent metal, 102 at. ppm (50 wt. ppm) weld zones	Table 2-1
Max interaction energy between P solute and dislocation	U_P^{max}	8 220 J/mol	(Sandström and Andersson 2008a, b)
Grain size	d_{grain}	See Table 7-1	
Reference yield strength	σ_{y0}	See Table 6-1	

5 Results from slow strain rate tensile tests

The measured yield strength values σ_{yexp} are listed in Table 5-1. These values have been determined with 0.2 % strain offset. For each test, the ring, the microstructure (weld zone), the temperature and strain rate are specified. Since there is a variation between different positions, it is the average value of the yield strength in different zones that is of interest. For this purpose a comparison to the model for the yield strength in Eq (4-19) is given. The model value of the yield strength is the stress where the stress strain model intersects the y-axis. A reference value of 75 MPa has been assumed for all zones to simplify the comparison. The model and the difference to the experimental values are given in Table 5-1. In the last column the average difference between the experiments and the model for each zone is given. For cross welds the average difference is about 10 MPa and for welds about 15 MPa. For HAZ only two tests are available for ring b, so the average value is taken for all specimens in this category, which gives 20 MPa. Thus in summary the average measured yield strength at the reference condition is 85 MPa for cross welds, 90 MPa for welds and 95 MPa for HAZ.

Table 5-1. Measured yield strengths and comparison to modelled values.

Micro-structure	Ring	Test	Temperature °C	Strain rate 1/s	σ_{yexp} MPa	Model σ_{ymod} MPa	$\sigma_{yexp}-\sigma_{ymod}$ MPa	$\sigma_{diff\ ave}$ MPa
Cross weld	a	T4	20	1×10^{-4}	75.1	75.0	0.1	
Cross weld	a	T3	20	3×10^{-6}	75.6	72.8	2.8	
Cross weld	a	T2	20	1×10^{-7}	72.5	70.7	1.8	
Cross weld	a	T9	75	1×10^{-4}	74.4	72.5	1.9	
Cross weld	a	T22	75	3×10^{-6}	73.3	69.6	3.7	
Cross weld	a	T11	75	1×10^{-7}	69.6	66.9	2.7	
Cross weld	a	T14	125	1×10^{-4}	84.1	69.1	15.0	
Cross weld	a	T24	125	3×10^{-6}	85.8	65.5	20.3	
Cross weld	a	T17	175	1×10^{-4}	80.1	65.6	14.5	
Cross weld	a	T27	175	3×10^{-6}	83.4	61.1	22.3	10.5
Cross weld	a	T32	125	1×10^{-7}	92.9	62.1	30.8	
HAZ	a	T6	20	1×10^{-4}	93.3	75.0	18.3	
HAZ	a	T20	20	3×10^{-6}	72.9	72.8	0.1	
HAZ	a	T12	75	1×10^{-4}	92.7	72.5	20.2	
HAZ	a	T21	75	3×10^{-6}	98.4	69.6	28.8	
HAZ	a	T31	75	1×10^{-7}	92.9	66.9	26.0	
HAZ	a	T25	125	3×10^{-6}	82.1	65.5	16.6	
HAZ	a	T18	175	1×10^{-4}	77.7	65.6	12.1	17.4
Weld	a	T5	20	1×10^{-4}	82.7	75.0	7.7	
Weld	a	T7	20	3×10^{-6}	81.6	72.8	8.8	
Weld	a	T8	20	1×10^{-7}	77.6	70.7	6.9	
Weld	a	T10	75	1×10^{-4}	76.9	72.5	4.4	
Weld	a	T23	75	3×10^{-6}	78.7	69.6	9.1	
Weld	a	T13	75	1×10^{-7}	83.0	66.9	16.1	
Weld	a	T16	125	1×10^{-4}	86.4	69.1	17.3	
Weld	a	T26	125	3×10^{-6}	89.5	65.5	24.0	
Weld	a	T19	175	1×10^{-4}	85.3	65.6	19.7	
Weld	a	T29	175	3×10^{-6}	84.8	61.1	23.7	13.8
Parent metal	b	T(6)	20	1×10^{-4}	76.2	75.0	1.2	
Parent metal	b	T(13)	75	1×10^{-4}	67.2	72.5	–5.3	
Parent metal	b	T(16)	125	1×10^{-4}	68.1	69.1	–1.0	–1.7
Cross weld	b	T(5)	20	3×10^{-6}	88.7	72.8	15.9	
Cross weld	b	T(9)	75	3×10^{-6}	78.3	69.6	8.7	
Cross weld	b	T(14)	125	3×10^{-6}	73.1	65.5	7.6	10.7
HAZ	b	T(4)	20	3×10^{-6}	102.3	72.8	29.5	
HAZ	b	T(11)	75	3×10^{-6}	96.3	69.6	26.7	28.1
Weld	b	T(7)	20	1×10^{-4}	92.9	75.0	17.9	
Weld	b	T(2)	20	3×10^{-6}	89.4	72.8	16.6	
Weld	b	T(8)	75	3×10^{-6}	87.2	69.6	17.6	
Weld	b	T(17)	125	3×10^{-6}	83.7	65.5	18.2	17.6

Examples of the temperature dependence of the flow curves are given in Figure 5-1 to Figure 5-3 for weld metal (thermo-mechanical affected zone, TMAZ), heat affected zone (HAZ), and cross welds. The true stress versus strain curves are presented. The curves are given up to the uniform elongation for the strain rate 1×10^{-4} 1/s. Results from the two rings are presented. In the legend box they are marked a and b, respectively. In four of the six diagrams the strength of the two rings can be compared for identical test conditions. It is evident that the strength of ring b is slightly higher than for ring a. At low strains the difference is about 10 MPa and at larger strains 10 to 20 MPa.

There is a pronounced decrease in flow strength with increasing temperature for the three types of weld microstructures investigated. This decrease is particularly marked at larger strains. This influence can be followed more directly if the two rings are considered separately. However, this result is not fully consistent. There is variation in strength between individual specimens, probably partially due to the fact that they have not been extracted at fully equivalent positions in the weldments. This variation is easiest to observe at small strains where the temperature dependence is smallest. The magnitude of the variation can be 10 MPa. The temperature dependence of the flow curves is increased with increasing strain rate for all microstructures.

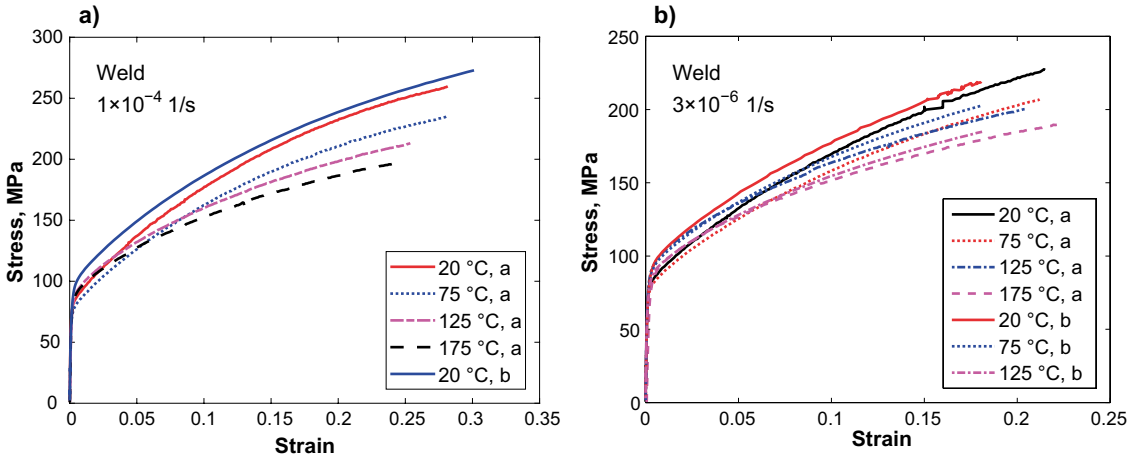

Figure 5-1. *Influence of temperature on the stress strain curves of weld zone specimens at strain rates a) 1×10^{-4} and b) 3×10^{-6} 1/s.*

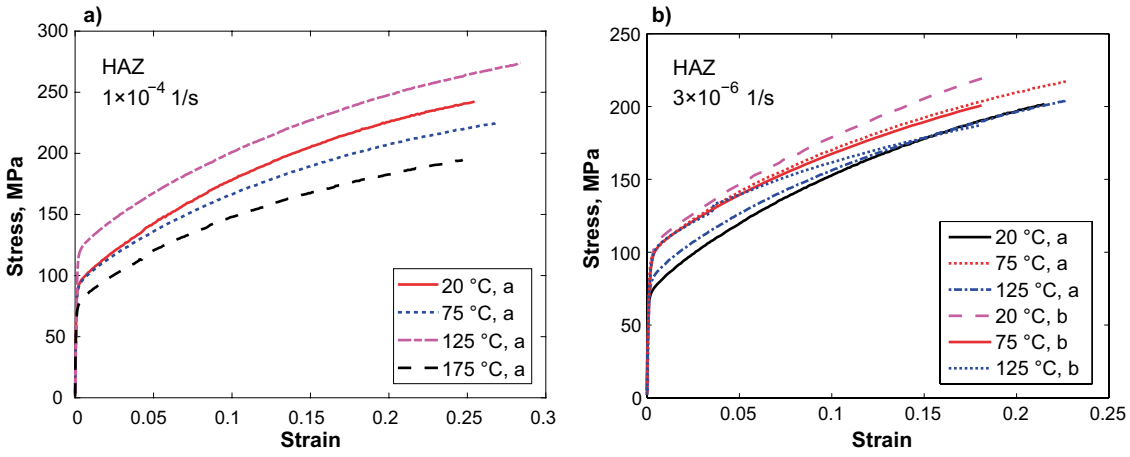

Figure 5-2. *Influence of temperature on the stress strain curves of heat affected zone (HAZ) specimens at strain rates of a) 1×10^{-4} and b) 3×10^{-6} 1/s.*

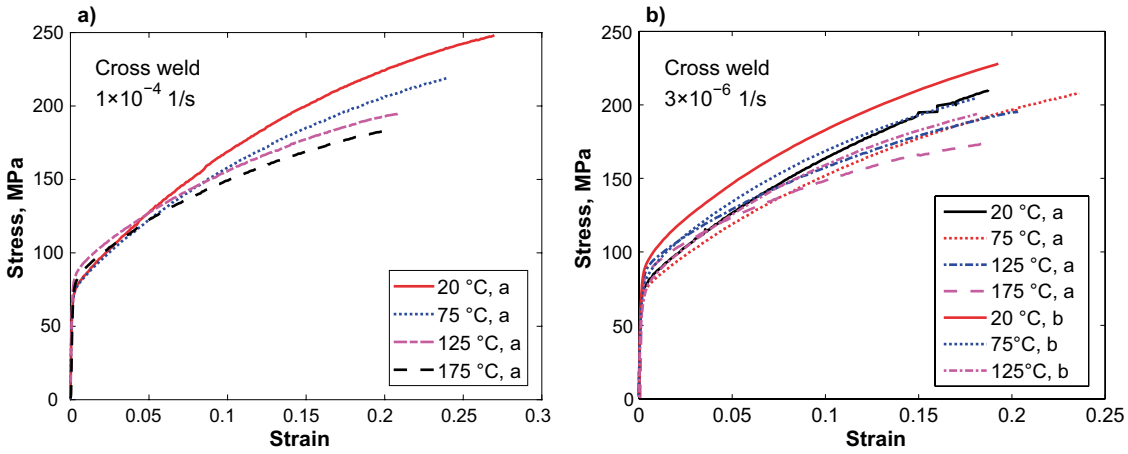

Figure 5-3. *Influence of temperature on the stress strain curves of cross weld specimens at strain rates of a) 1×10^{-4} and b) 3×10^{-6} 1/s.*

In Figure 5-4 to Figure 5-6 the strain rate dependence of the flow stress is illustrated. The strength is expected to increase with increasing strain rate, Eq (4-13), and that is also the general trend in the figures. The strain rate dependence gives a considerably smaller variation between the flow curves than the temperature dependence does. The strain rate dependence decreases somewhat with increasing temperature, although this effect is modest. The small influence of the strain rate means that curves from different strain rates cross each other in several cases. The influence of the strain rate is about the same for the weld metal, heat affected zone and the cross welds. From Figure 5-4 to Figure 5-6 the difference between ring a and b is easily discernible. The strength of ring b is in general somewhat higher than for ring a.

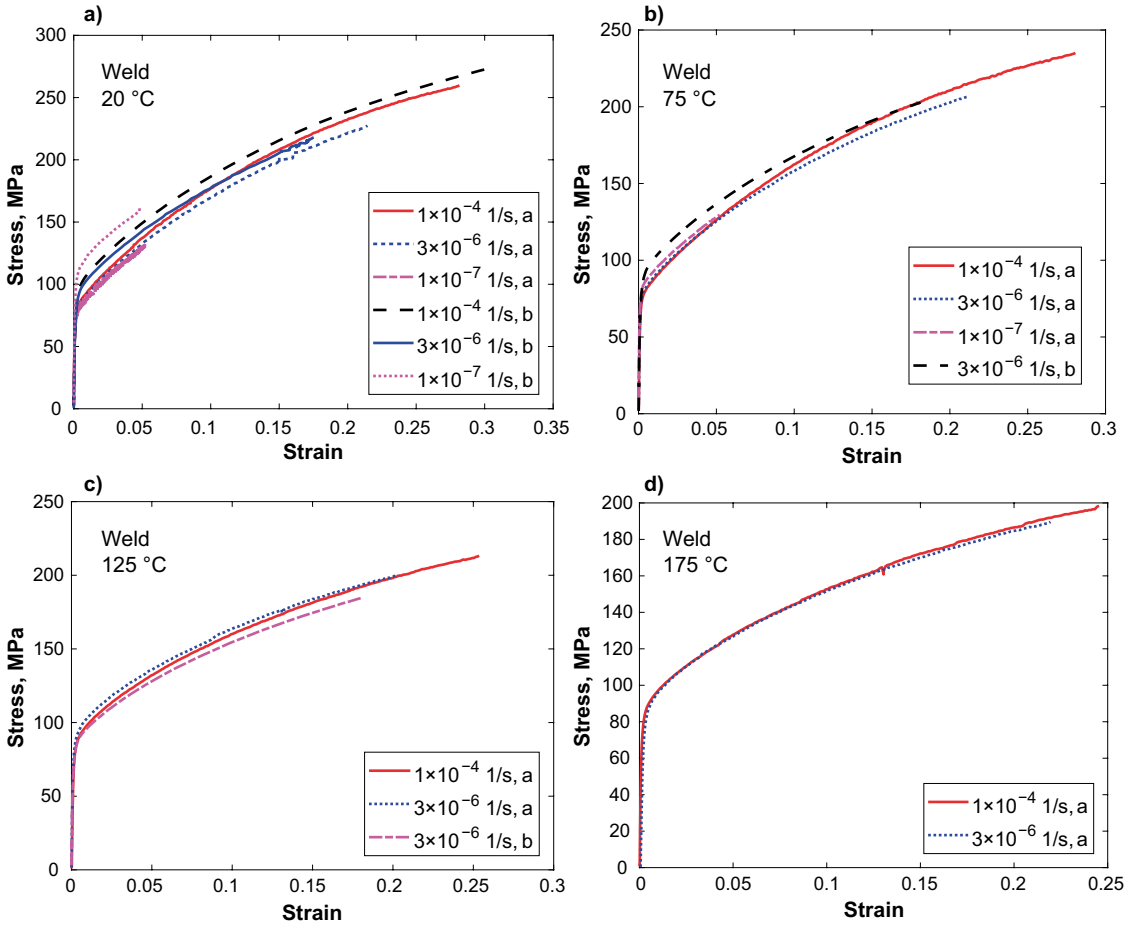

Figure 5-4. *Influence of strain rate on the stress strain curves of weld zone specimens at temperatures of a) 20 °C, b) 75 °C, c) 125 °C, d) 175 °C.*

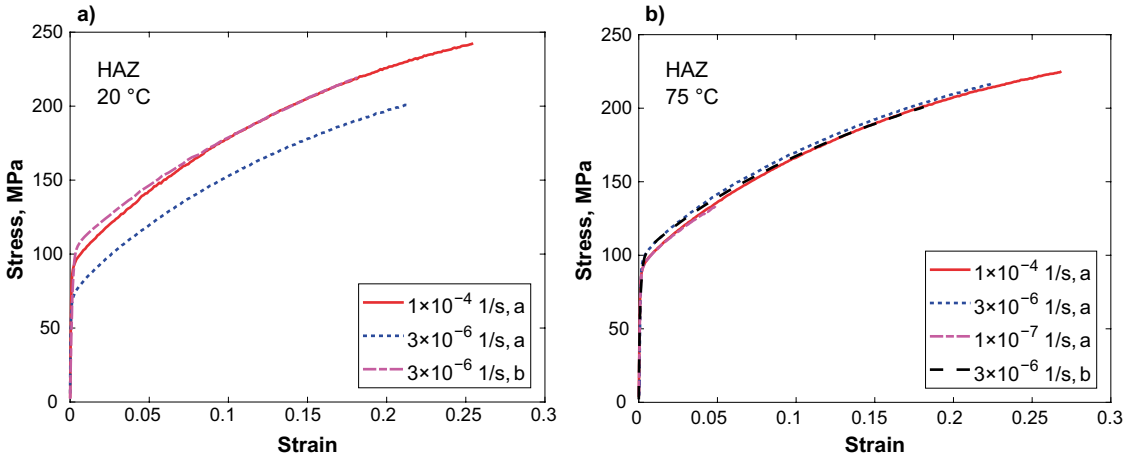

Figure 5-5. *Strain rate dependence of stress strain curves for HAZ specimens at temperatures of a) 20 °C and b) 75 °C.*

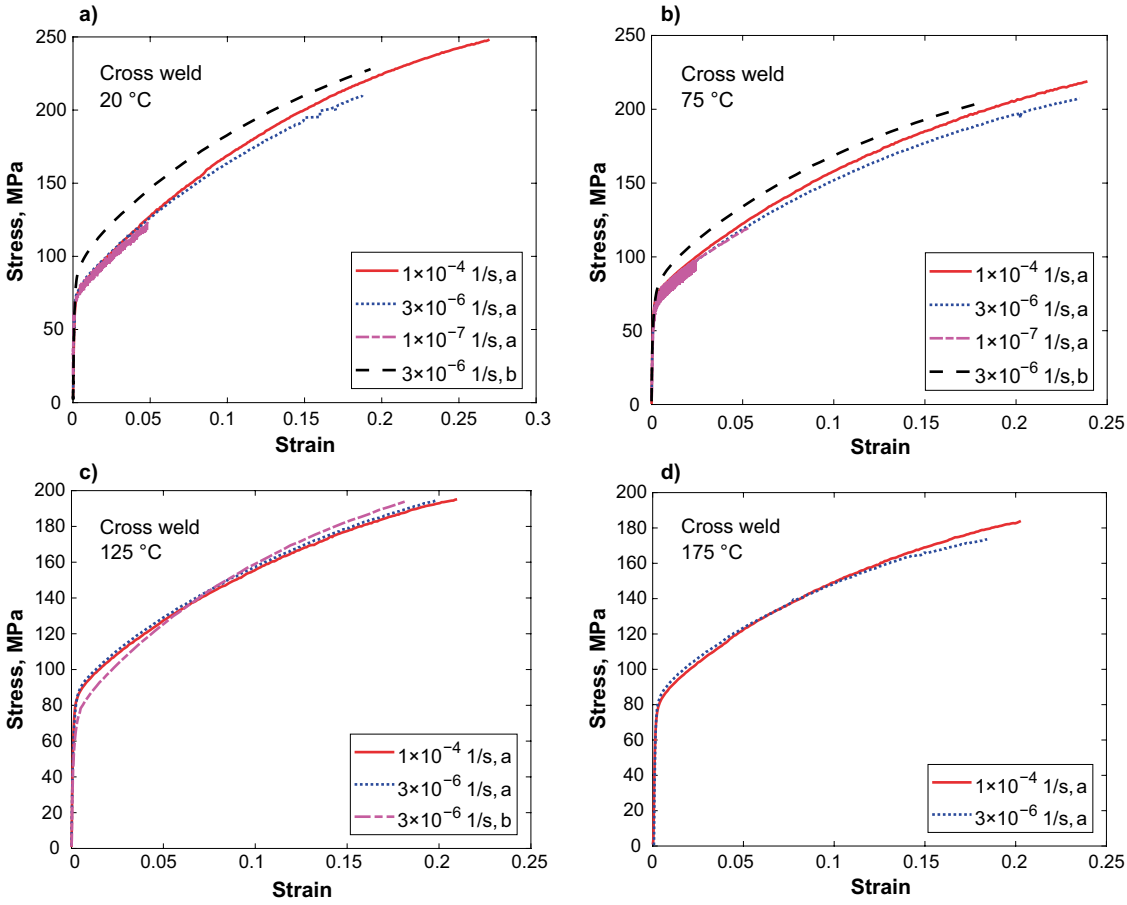

Figure 5-6. *Strain rate dependence of stress strain curves for cross weld specimens at temperatures of a) 20 °C, b) 75 °C, c) 125 °C, d) 175 °C.*

In Figure 5-7 to Figure 5-10 the various weld microstructures are compared for a given strain rate and temperature. In Figure 5-7 and Figure 5-8a base metal curves are available both from lid material in Sandström and Hallgren (2012) and from ring b. Up to a strain of 0.2 the curves are almost identical. The ductility of ring b is somewhat higher than for the material investigated in Sandström and Hallgren (2012) (not shown). The closeness of the curves for the two heats of parent metals up to the point of necking has important implications. This means that there is no dependence of the position where the parent metal specimens were extracted. The variation that is found for the weld specimens should therefore be considered to be intrinsic.

In Figure 5-7 to Figure 5-10 the stress strain curves for the different weld zones can be compared. The base metal has in most cases the lowest yield strength. At the same time its work hardening rate is higher than for the weld zones. This implies that the difference between the base metal and the weld zones decreases with increasing strain. No systematic ranking in strength between weld, HAZ, and cross weld can be observed. It seems that position in the individual zone plays an equally important role. In some cases the cross welds have a lower ductility than the weld metal and HAZ (not shown). Even if there is no systematic strength difference between the weld zones, local variations in strength differences increase the possibility of early necking and thereby a reduction of elongation. There is some tendency that the difference between the zones with respect to strain rate is reduced at higher temperatures.

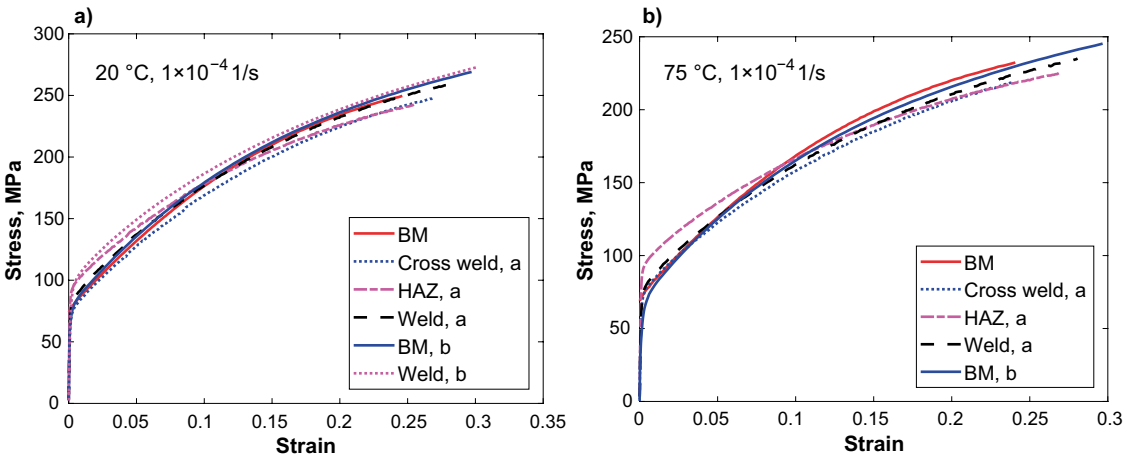

Figure 5-7. *Comparison of stress strain curves for different weld zones at 1×10^{-4} 1/s. a) 20 °C, b) 75 °C.*

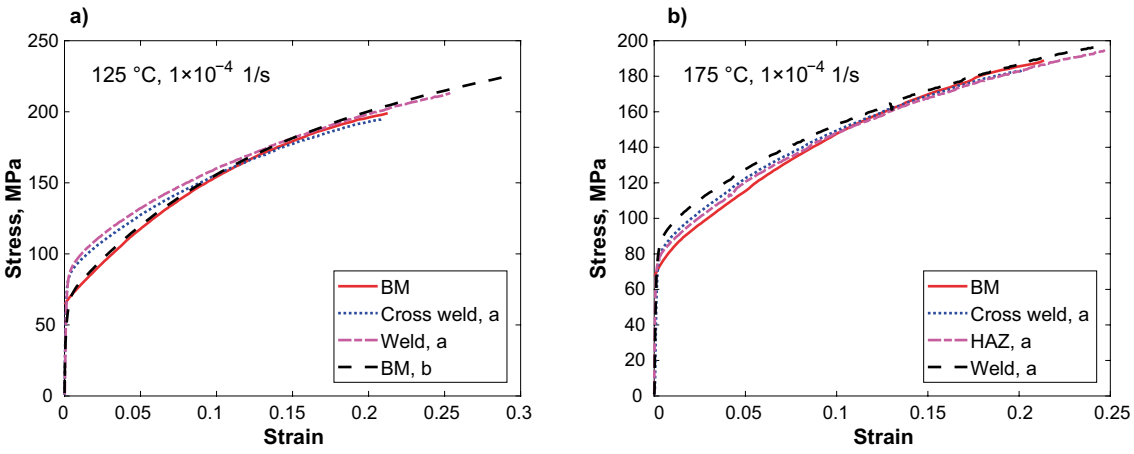

Figure 5-8. *Comparison of stress strain curves for different weld zones at 1×10^{-4} 1/s. a) 125 °C, b) 175 °C.*

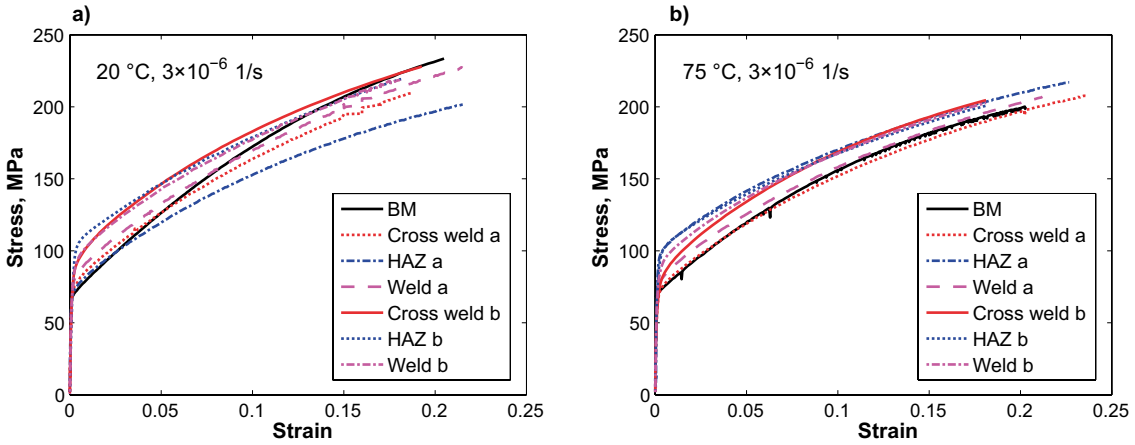

Figure 5-9. *Comparison of stress strain curves for different weld zones at 3×10^{-6} 1/s. a) 20 °C, b) 75 °C.*

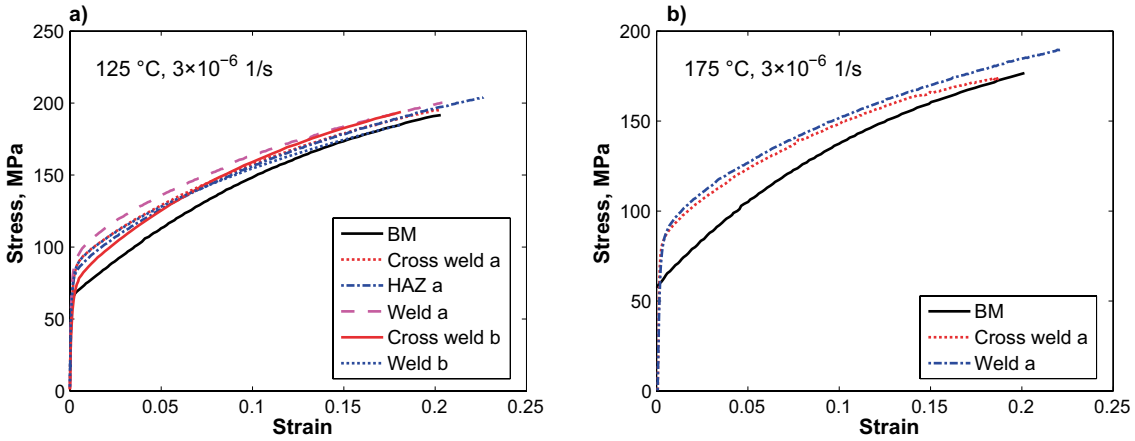

Figure 5-10. *Comparison of stress strain curves for different weld zones at 3×10^{-6} 1/s. a) 125 °C, b) 175 °C.*

6 Model results for stress strain curves

The parameters used in the models are given in Table 4-1. There is, however, one parameter that cannot be determined from basic principles and that is the reference value of yield strength, i.e. the value at the reference condition 20 °C and 1×10^{-4} 1/s. For this reason experimental values are used for this quantity. Once the reference value is given, the temperature and strain rate dependence of the yield strength can be determined with the help of Eq (4-19). The reference values found from the experimental stress strain curves are listed in Table 6-1. To determine the reference values, each experimental yield strength is transferred to the reference condition with the help of Eq (4-19), and then the average value is taken for a specific weld zone. Two values for each microstructure (weld zone) are listed. The first one is derived from Table 5-1, where the values are obtained with a conventional strain offset method for the yield strength. The second one is taken from the full flow curves at zero strain. On average the latter ones are about 5 MPa higher. The upper and lower limits are determined from the variation in the values from the full flow curves.

Table 6-1. Values of the yield strength at the reference condition 20 °C and 1×10^{-4} 1/s.

Ring	Weld microstructure	Reference yield strength from measurements, MPa	Reference yield strength from flow curves, MPa	Lower limit, MPa	Upper limit, MPa
0	Parent metal (Sandström and Hallgren 2012)	75	75	70	77
a	Weld	89	95	90	105
a	HAZ	92	95	80	105
a	Cross weld	85	90	80	105
b	Parent metal	73	75	70	77
b	Weld	93	100	100	100
b	HAZ	103	105	103	105
b	Cross weld	86	100	90	100

As can be seen from Table 6-1, the yield strength in the weld zones is higher than in the parent metal. Furthermore the yield strength is slightly higher in the weld zones for ring b than for ring a. The difference is 5, 10, and 10 MPa for weld, HAZ and cross welds. Since there is variation in the observed yield strength between different specimens, a lower and an upper limit for the reference value is given in Table 6-1. The difference between the upper and lower limits varies from nothing up to 25 MPa depending on weld zone and ring. For the parent metal the variation is smaller and should be considered as normal scatter in the test results. In the modelling it is the reference yield strength from the flow curves that is applied.

Using the model in Section 4.2, Eq (4-16), the parameter values in Table 4-1 and the yield strength reference values in Table 6-1, the stress strain curves can be computed. To illustrate the validity of the model, examples are first given for parent metal with experimental data from Sandström and Hallgren (2012). In Figure 6-1 the temperature dependence of the flow curves and in Figure 6-2 the influence of the strain rate are shown. Experimental curves for strains up to the uniform elongation are given. The agreement between experiments and predictions demonstrates the validity of the model. Since necking is not taken into account in the model, comparison to data points beyond the maximum in the experimental flow curves is meaningless.

Examples of results for the weld zone are given in Figure 6-3 and compared to the measured curves: The model can reproduce the observations in an acceptable way.

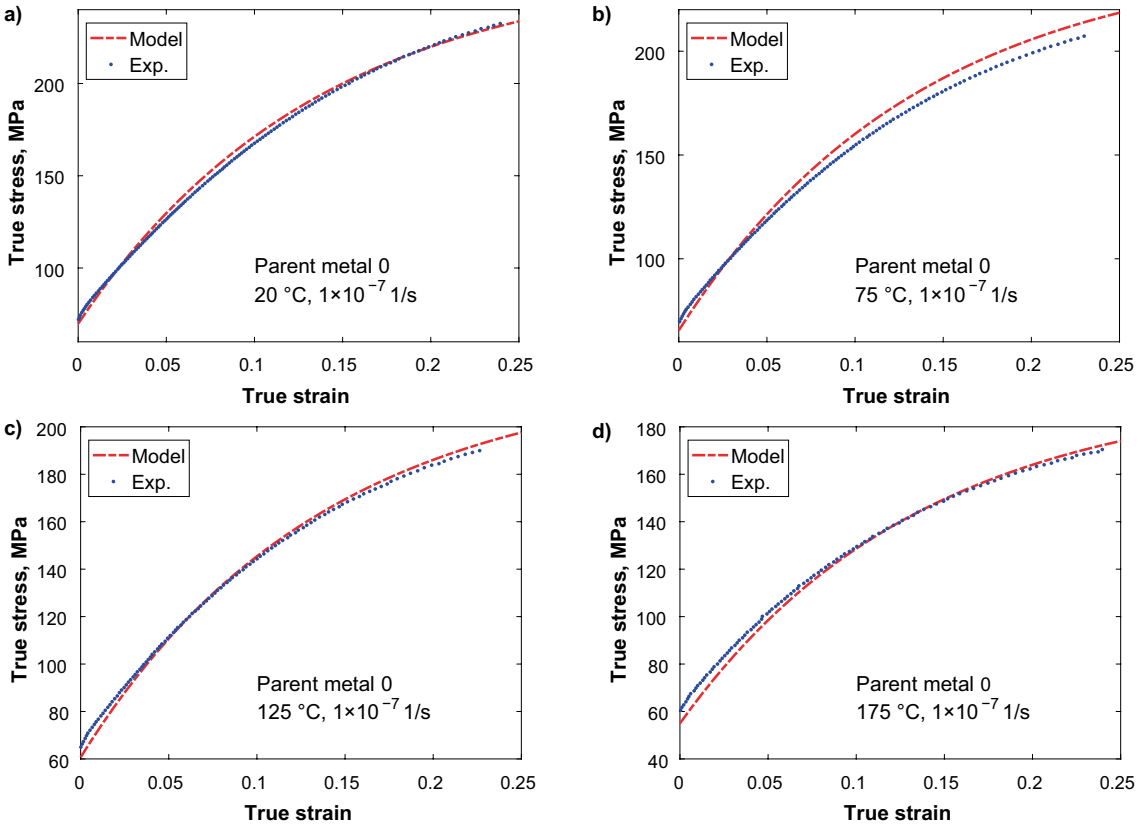

Figure 6-1. *Influence of temperature. Comparison of experimental and model stress strain curves, Eq (4-16), for parent metal with data from Sandström and Hallgren (2012);. a) 20 °C, 1×10^{-7} 1/s, ring 0; b) 75 °C, 1×10^{-7} 1/s, ring 0; c) 125 °C, 1×10^{-7} 1/s, ring 0; d) 175 °C, 1×10^{-7} 1/s, ring 0.*

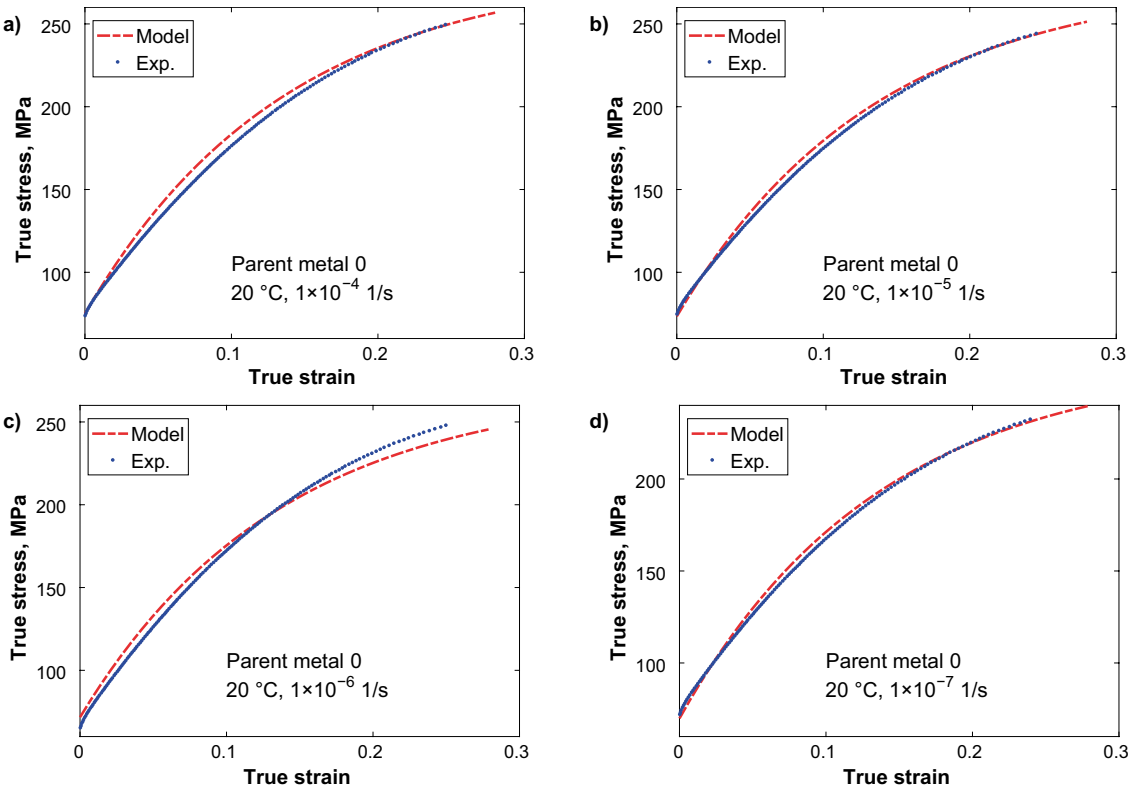

Figure 6-2. *Influence of strain rate. Comparison of experimental and model stress strain curves, Eq (4-16), for parent metal with data from Sandström and Hallgren (2012);. a) 20 °C, 1×10^{-4} 1/s, ring 0; b) 20 °C, 1×10^{-5} 1/s, ring 0; c) 20 °C, 1×10^{-6} 1/s, ring 0; d) 20 °C, 1×10^{-7} 1/s, ring 0.*

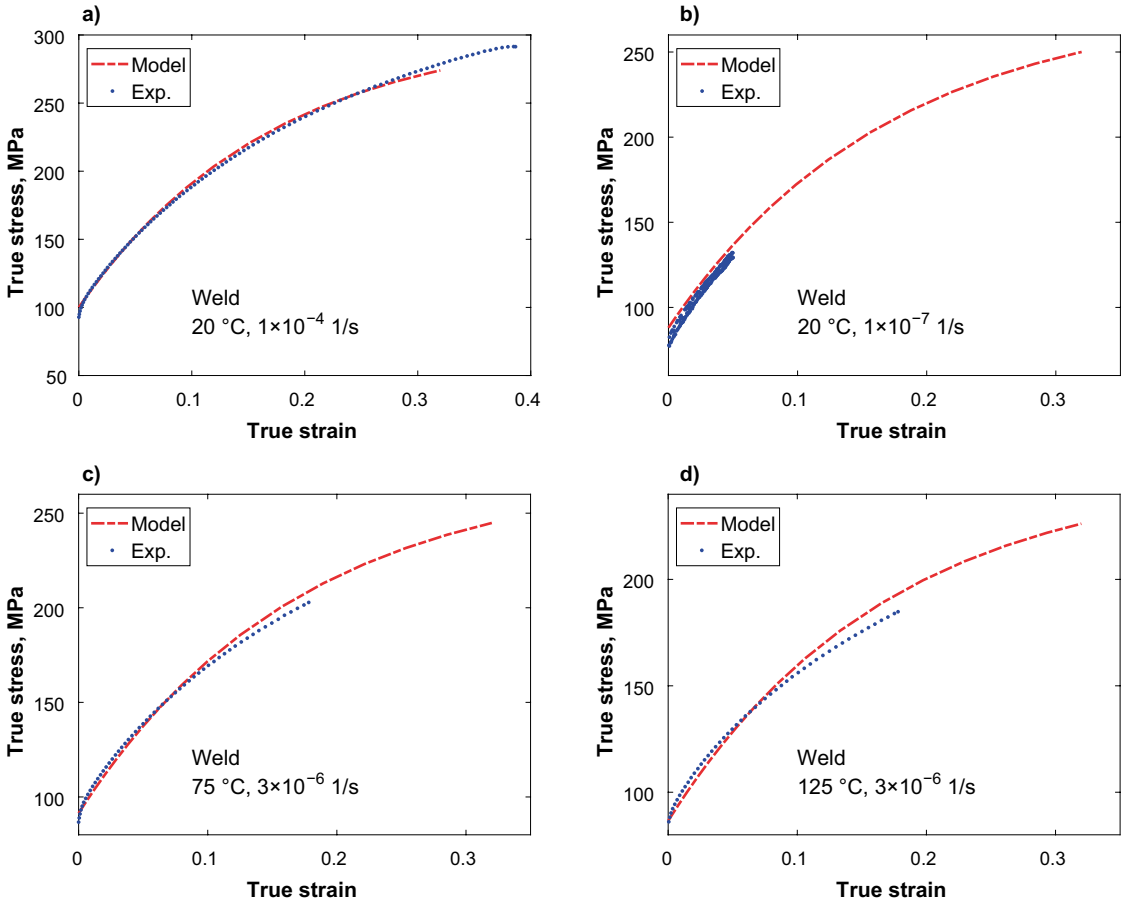

Figure 6-3. *Comparison of experimental and model stress strain curves Eq (4-16), for the weld (TMAZ);. a) 20 °C, 1 × 10⁻⁴ 1/s, ring b; b) 20 °C, 1 × 10⁻⁷ 1/s, ring a; c) 75 °C, 3 × 10⁻⁶ 1/s, ring a; d) 125 °C, 3 × 10⁻⁶ 1/s, ring b.*

To simplify the application of the model, the details of the computation for one case will be given, namely for the curve in Figure 6-3c. To describe the curve three parameters are needed ω, σ_y and K, cf. Eq (4-16).

We find ω from Eq (4-4). With $m = 3.06$, $b = 2.56 \times 10^{-10}$ m (not actually needed), $d_{int} = 2\,b$ for the weld zones, and $n_{slip} = 12$, we get ω = 11.73. The value of K is obtained from Eq (4-15). The parameters in this equation are known except for c_L, which is found from Eqs (4-13) and Eq (4-17) by iteration. The resulting value is $c_L = 36.7$. At 75 °C, $G = 43\,627$ MPa, see Table 4-1. With Eq (4-15) this gives $K = 180.2$ MPa. Values for K and c_L can also be obtained from Tables A-1b and A-2b in the Appendix. For parent metal with ω = 14.67, the corresponding values are listed in Tables A-1a and A-2a.

To find the third parameter, the yield strength, the creep exponent (Norton exponent) must first be determined. This exponent is evaluated at the stationary creep stress σ_{stat}. This stress satisfies Eq (4-21)

$$\dot{\varepsilon} = h(\sigma_{stat}, T) \qquad \text{Eq (6-1)}$$

for the investigated case $\dot{\varepsilon} = 3 \times 10^{-6}$ and $T = 75$ °C. Solving Eq (6-1) by iteration gives $\sigma_{stat} = 180.2$ MPa. In fact, $\sigma_{stat} = K$ and can be taken from Table A-1b. A small variation of stress around σ_{stat} is applied to obtain the creep exponent n_N

$$n_N = \frac{\log(h(\sigma_{stat}(1+\delta), T) / h(\sigma_{stat}(1-\delta), T))}{\log((1+\delta)/(1-\delta))} \qquad \text{Eq (6-2)}$$

The natural logarithm can be used in Eq (6-2). δ is any sufficiently small number, for example 0.01. The resulting creep exponent is 67.4. Values for other temperatures and strain rates can be found in Table A-3. The ratio between the yield strength and its reference value can now be determined from Eq (4-19). $G(T_0)$ = 45 400 and G(75 °C) = 43 627 MPa, see Table 4-1. The resulting ratio is 0.909 and with the reference value σ_{y0} = 95 (Table 6-1), we find that σ_y = 86.4 MPa.

In Figure 6-4 the model and experimental values are compared for the heat affected zone (HAZ). Similarly in Figure 6-5 the corresponding comparison is made for cross welds.

In the report (Jin and Sandstrom 2013), a figure (Figure 2-1) was given for stress strain curves that were used in Finite Element (FEM) computations for the copper canister. This figure was based on preliminary results. An updated version is presented in Figure 6-6. It uses Eq (4-16) that can be rewritten as (where $\sigma_{max} = K + \sigma_y$ has been inserted).

$$\sigma = \sigma_y(T_0, \dot{\varepsilon}_0)\frac{\sigma_y(T, \dot{\varepsilon})}{\sigma_y(T_0, \dot{\varepsilon}_0)} + K(1 - e^{-\omega\varepsilon/2}) \qquad \text{Eq (6-3)}$$

The first term on the right hand side has been given as the reference yield strength multiplied by the yield strength ratio at a specified temperature and strain rate. In this way the Tables A-1, A-3 and A-4 in the Appendix can be applied directly.

In spite of the fact that the K value is higher for parent metal than for the weld zones (weld and HAZ), the weld zones give higher flow stresses due to the higher yield strength. The curve for the parent metal has a larger curvature than that for the weld zones due to the larger ω value. Curves for other yield strengths, temperatures and strain rates can be obtained directly with the help of Tables A-1, A-3 and A-4.

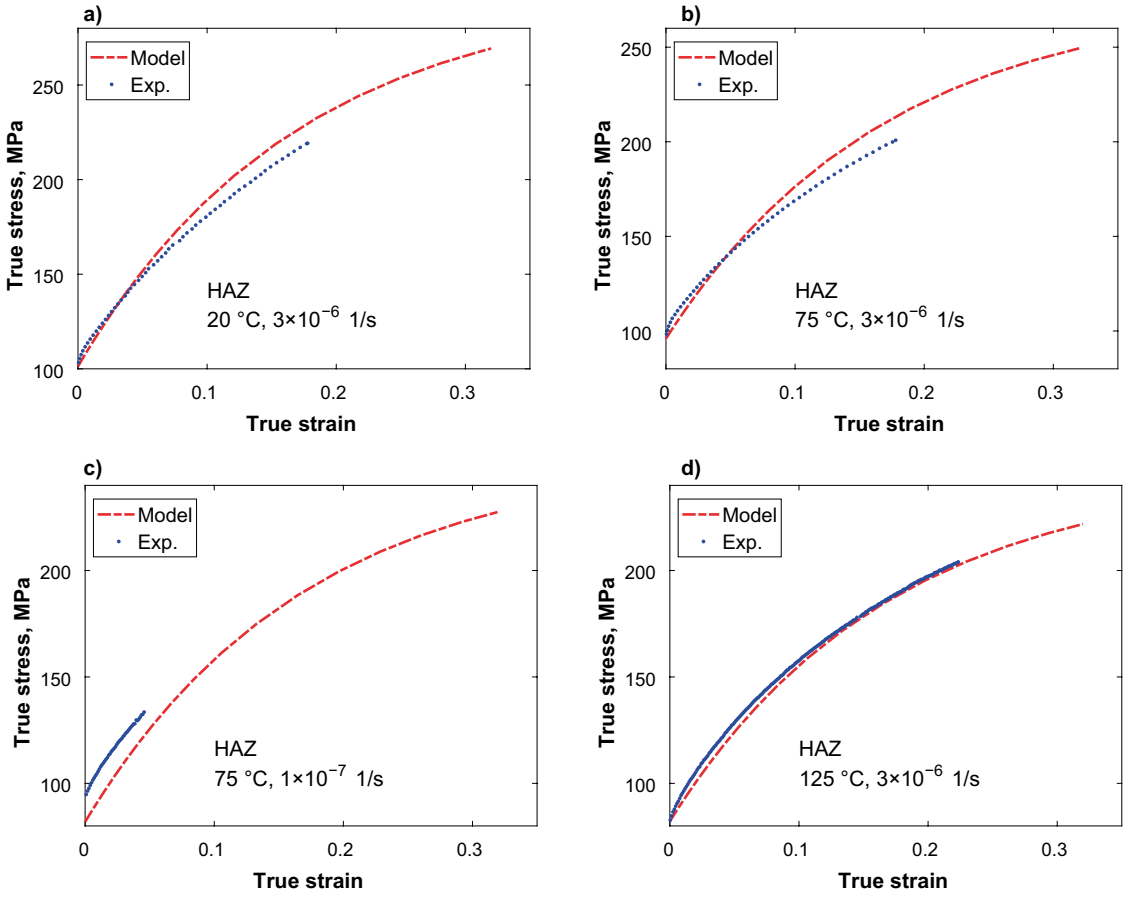

Figure 6-4. *Comparison of experimental and model stress strain curves Eq (4-16), for the heat affected zone;. a) 20 °C, 3 × 10⁻⁶ 1/s, ring b; b) 75 °C, 3 × 10⁻⁶ 1/s, ring b; c) 75 °C, 1 × 10⁻⁷ 1/s, ring a; d) 125 °C, 3 × 10⁻⁶ 1/s, ring a.*

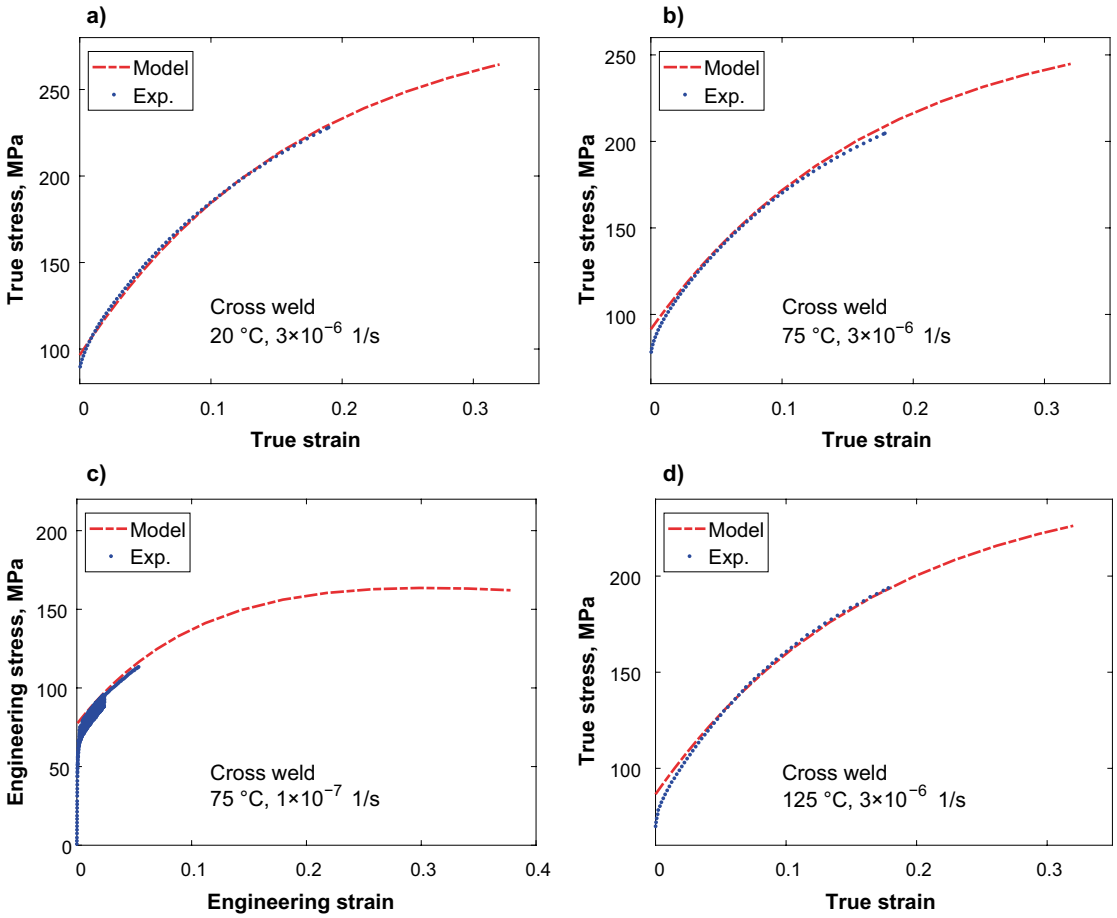

Figure 6-5. *Comparison of experimental and model stress strain curves Eq (4-16), for cross weld specimens;. a) 20 °C, 3×10^{-6} 1/s, ring b; b) 75 °C, 3×10^{-6} 1/s, ring b; c) 75 °C, 1×10^{-7} 1/s, ring a; d) 125 °C, 3×10^{-6} 1/s, ring b.*

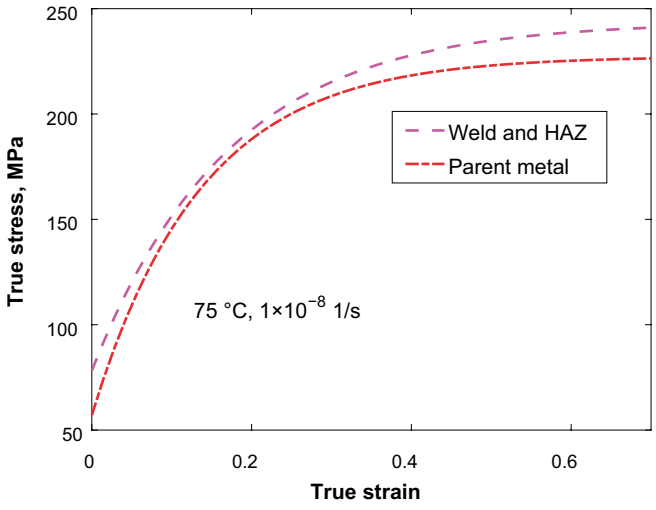

Figure 6-6. *Examples of stress strain curve for FEM, Eq (6-3). Parameter values: parent metal (σ_y = 57.0 MPa (σ_{y0} = 69 MPa), K = 171.0 MPa, ω = 14.67) and weld zones (σ_y = 78.1 MPa (σ_{y0} = 95 MPa), K = 165.5 MPa, ω = 11.73).*

7 Creep strain versus time curves

Eq (4-22) gives the time derivative of the creep strain, which can be integrated to find the creep strain versus time curve. This model has previously been applied to Cu-OFP parent metal (Sandström 2012). Some preliminary results for welds have also been presented (Sandström et al. 2013). In Sandström et al. (2013), however, the same parameters were used for parent metal and weld zones except for the yield strength. The purpose here is to apply the same parameters as were used for the slow strain rate tensile tests. The start Eq (4-7) should be applicable to different types of plastic deformation and the same parameter values should be used in different situations for the equation to make sense, independently whether strain rate or load controlled tests are considered. The creep data for friction stir welded Cu-OFP is taken from Andersson et al. (2007).

The yield strengths at reference condition that are used in the computations for the creep curves are given in Table 7-1.

Table 7-1. Yield strengths at the reference condition 20 °C, 1×10^{-4} 1/s.

Microstructure	Grain size µm	Reference yield strength σ_{y0} MPa
Parent metal tube	100	69
Parent metal lid	70	74.8
Weld metal	200	95
HAZ	400	95
Cross weld	400	90

For the parent metal the lower grain size in the lid in comparison to the tube gives a higher yield strength. The values of the yield strength in the weld zones might seem high. It should be recalled that the values are taken from the flow curve for zero plastic strain and that value is typically about 5 MPa higher than the yield strength measured in the conventional way with a strain offset, see Table 6-1. The cross welds are handled in the same way as the other weld zones. In principle, the contributions from parent metal, weld and heat affected zone should be added. Such an analysis has been performed but the results are almost identical so this complication is not considered here.

Examples of creep curves for annealed Cu-OFP is illustrated in Figure 7-1 together with modelling values with Eq (4-22) and Eq (4-27). The creep curves have been determined from annealed material taken from a canister lid (Andersson-Östling and Sandström 2011). The annealing treatment was 5 minutes at 600 °C followed by water quenching.

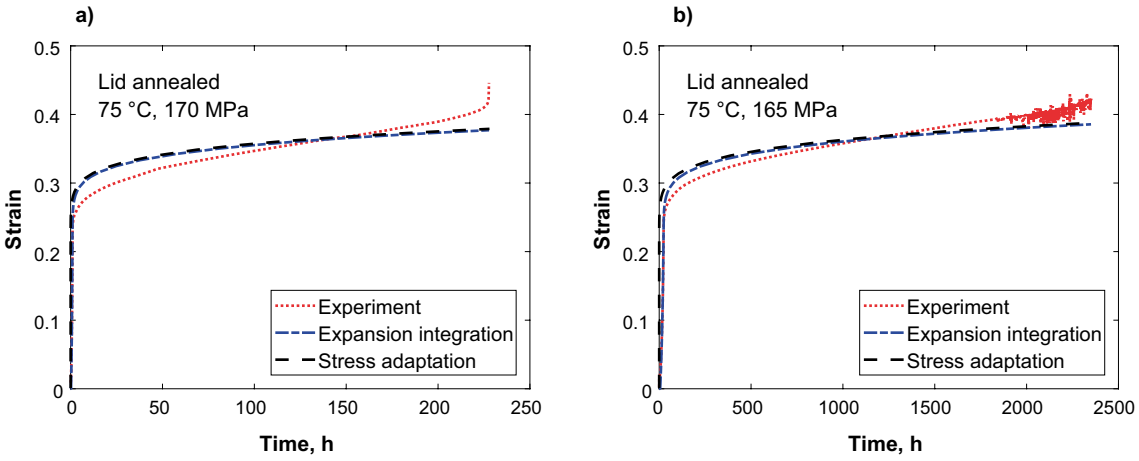

Figure 7-1. *Comparison of experimental and model creep curves for annealed parent metal. Model results for stress adaptation, Eq (4-22) and expansion integration, Eq (4-27) are shown. Experiments from Andersson-Östling and Sandström (2011); a) 75 °C, 170 MPa; b) 75 °C, 165 MPa.*

It is evident that the primary creep model can describe the creep curves for annealed Cu-OFP quite well. It can also be seen that the numerical alternative expansion integration gives virtually identical results to stress adaptation, the most direct way of solving the differential equation.

For annealed Cu-OFP the yield strength is about 35 MPa. However, for material that has not been annealed the yield strength is much higher, for parent metal about 70 MPa, see Table 7-1. It is well known that cold work can have a dramatic effect and reduce the creep rate many orders of magnitude (Sandström 2016c, Wu et al. 2014). Even a small amount of cold work in a material that has not been annealed reduces the creep rate. It is described in Sandström (2016c) how this can be handled in the modelling. The difference in yield strength between annealed and as delivered (not annealed) material gives rise to a contribution to the strain on loading. By solving for the strain in Eq (4-16), the following expression for the strain on loading ε_{init} is obtained

$$\varepsilon_{\text{init}} = -\frac{2}{\omega}\log\left(1-\frac{\sigma_{\text{appl}}-\sigma_y(\dot{\varepsilon},T)}{K(\dot{\varepsilon},T)}\right) \qquad \text{Eq (7-1)}$$

σ_{appl} is the applied creep stress. The difference in loading strain between the annealed and the as delivered state can then be found by inserting the appropriate values in Eq (7-1)

$$\Delta\varepsilon_{\text{init}} = \varepsilon_{\text{init anneal}} - \varepsilon_{\text{init as del}} \qquad \text{Eq (7-2)}$$

$\Delta\varepsilon_{init}$ is introduced in the equation for the creep rate, Eq (4-22)

$$\frac{d\varepsilon}{dt} = h(\sigma_{\text{y}}(T,\dot{\varepsilon}) + \frac{\sigma-\sigma_{\text{y}}(T,\dot{\varepsilon})}{1-e^{-\omega(\varepsilon+\Delta\varepsilon_{init})/2}}, T) \qquad \text{Eq (7-3)}$$

Results for parent metal that has not been annealed are illustrated in Figure 7-2 using Eq (7-3). Extruded material can be found in the canister tube and forged material in the canister lid and bottom. With the help of the modification in Eq (7-3), creep curves for as delivered Cu-OFP can be represented.

The cusps in the experimental creep curves are due to the necessity of reloading the creep machine when a certain strain has been reached.

Since the weld zones have even higher yield strengths than the as delivered parent metal, Eq (7-3) will be applied to the weld zones as well. Computations are compared to experiments for HAZ in Figure 7-3, for weld metal in Figure 7-4 and for cross welds in Figure 7-5.

To make it easier to apply the models, some numerical details will be given. The first case is the integration of the max stress integration. The case in Figure 7-3a will be considered. Inserting the temperature 75 °C and creep stress 170 MPa in Eq (4-19) gives the stationary strain rate 4.6×10^{-8} 1/s and Eq (6-2) the creep exponent n_N = 59.9. In the same way as above in Chapter 6, the value of K = 170 MPa is obtained from Eq (4-15). It is equal to the applied stress. The parameter c_L is found from Eq (4-13) and Eq (4-17) by iteration. The resulting value is c_L = 38.9. The value can also be found from Table A-2b by interpolation. At 75 °C, G = 43 630 MPa. With G and $\dot{\varepsilon}$ known and the reference yield strength = 95 MPa taken from Table 7-1, the yield strength σ_y = 80.7 MPa can be obtained, see also Table A-4b. All the parameters in Eq (7-3) are now known and the integration can be performed directly.

Results from all the three approaches of numerically solving Eq (4-22) described in Section 4.5 with the modification in Eq (7-3) are shown in Figure 7-3 to Figure 7-5. The three ways of integrating the equation for primary creep Stress adaptation, Eq (4-22), Expansion integration, Eq (4-27), and Max stress integration Eq (4-34) give similar results and in most practical applications any of the methods can be used.

An acceptable representation of the experimental data for the different weld zones have been obtained. The model takes primary and secondary creep into account but not tertiary creep. Consequently it is only meaningful to compare results for the primary and secondary stage. Even the creep curves for the cross-weld specimens have been reproduced in a satisfactory way. This is gratifying since the behaviour of the complex microstructure in cross-welds is often difficult to describe.

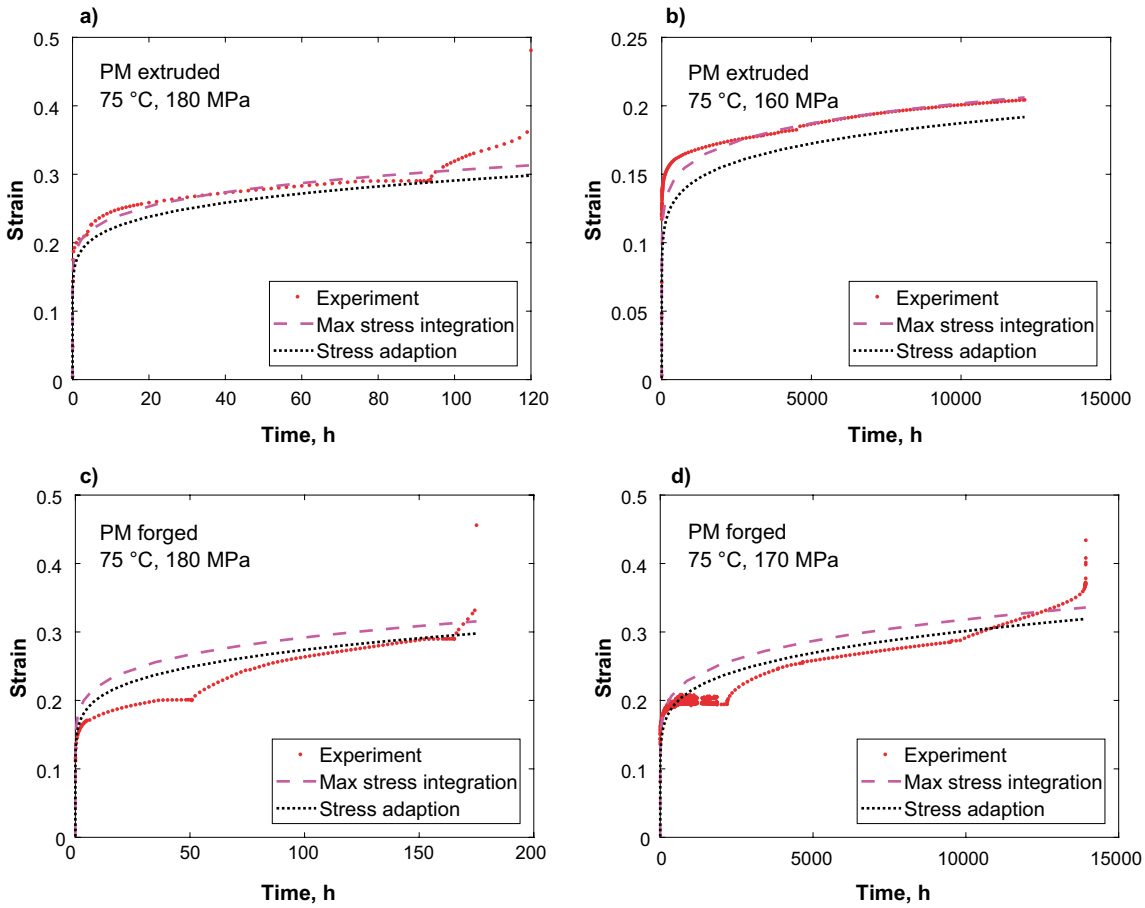

Figure 7-2. *Comparison of experimental and model creep curves for parent metal;. Experiments from Andersson et al. (2007); a) 75 °C, 180 MPa; b) 75 °C, 160 MPa; c) 75 °C, 180 MPa; d) 75 °C, 170 MPa.*

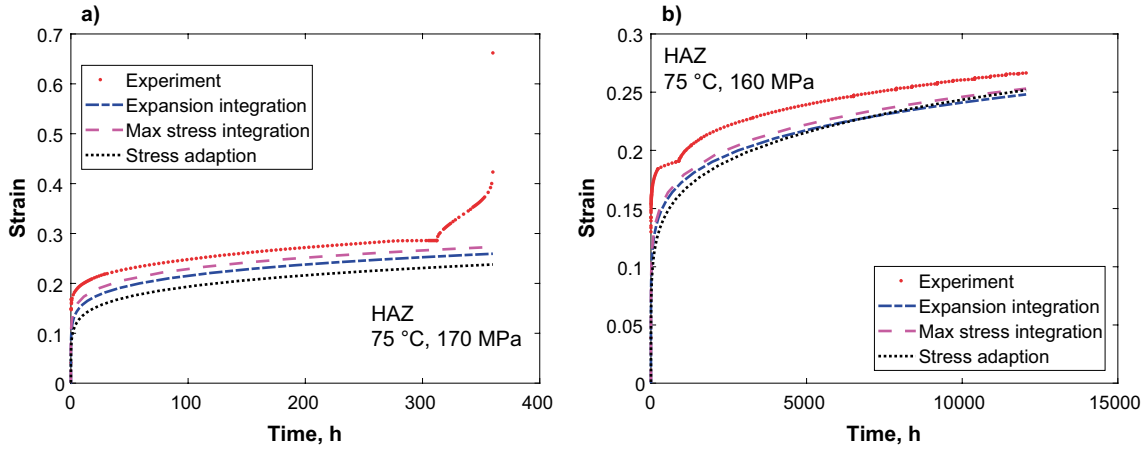

Figure 7-3. *Comparison of experimental and model creep curves for the heat affected zone. Experiments from Andersson et al. (2007); a) 75 °C, 170 MPa; b) 75 °C, 160 MPa.*

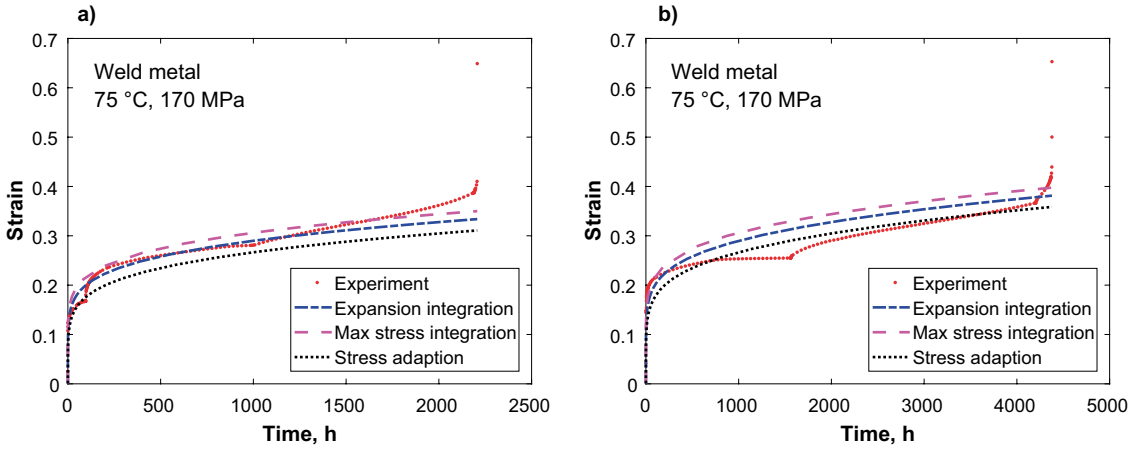

Figure 7-4. *Comparison of experimental and model creep curves for the weld metal. Experiments from Andersson et al. (2007); a) 75 °C, 170 MPa; b) 75 °C, 170 MPa.*

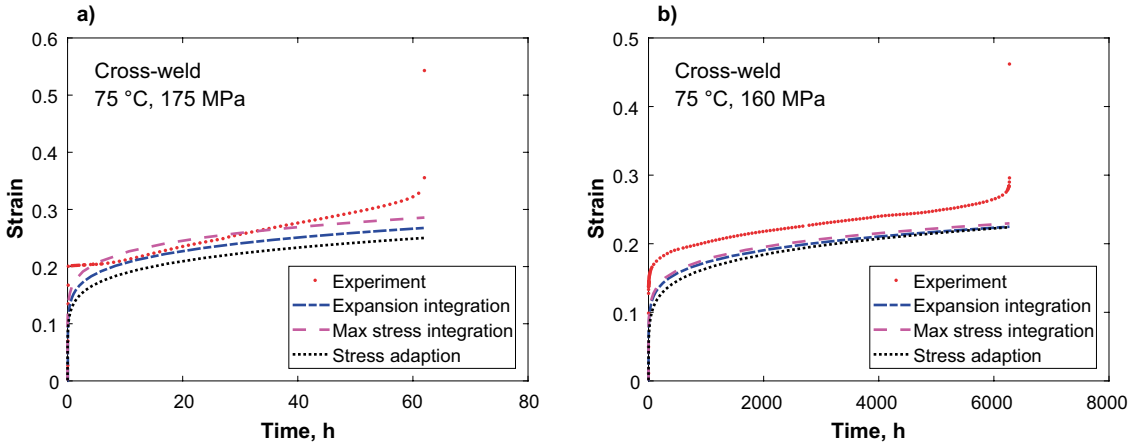

Figure 7-5. *Comparison of experimental and model creep curves for cross-weld specimens;. Experiments from Andersson et al. (2007); a) 75 °C, 175 MPa; b) 75 °C, 160 MPa.*

8 Discussion

Slow rate tensile tests have been performed for the weld zone and heat affected zone (HAZ) in friction stir welded Cu-OFP. In addition, cross weld samples have been extracted and tested. The results show that the flow curves of the different zones in the welds lie somewhat above those of the base metal at low strains. Thus, the weld zones have higher yield strength than the parent metal. Most base metal data have been taken from Sandström and Hallgren (2012). The work hardening of the parent metal is typically higher than that of the weld zones. This implies that sometimes the flow curves cross. The influence of weld microstructure seems to decrease with increasing temperature and decreasing strain rate. It is a common experience that the influence of the microstructure in general tend to decrease at higher temperatures and longer testing times (= lower strain rate), since a homogenisation of the microstructure takes place in parallel to the creep deformation.

All the weld microstructures show a high ductility. At 20 and 75 °C and 1×10^{-4} 1/s, the elongation is about 40 %, Figure 5-7. At the same strain rate but at the higher temperatures the cross welds have a somewhat lower elongation of about 30 %, which is less than for the weld zone and the HAZ specimens. At the lower strain rates the specimens have not been tested to rupture and the elongation at rupture has consequently not been possible to measure. However, it can be seen from the flow curves at 3×10^{-6} 1/s that the elongation is well above 20 %.

A variation in the yield strength and the flow curves for weld zones has been observed. This is not believed to be simple scatter in the test data. The reason is that little scatter is observed between the parent metal specimens. Thus, there seems to be an intrinsic variation between different positions in the weld.

Two welded rings were studied. It was originally assumed that the welding procedures for the two rings were essentially identical. However, it has turned out that ring a was welded in air and ring b with argon as shielding gas. The yield strength measured both directly with the intercept method or from extrapolation of the flow curves to zero strain was 5 to 10 MPa higher for ring b than for ring a. This difference is small in comparison to the intrinsic variations in the strength in the weld zones. It is therefore difficult to ascertain any significant influence of the welding procedure.

Basic constitutive equations have been developed for the different zones in the friction stir welds. Constitutive equations both for stress strain flow curves as well as for creep time strain curves have been formulated. An important parameter in the models is the interaction distance between dislocations for them to be able combine and form low energy configurations during deformation. To reflect the more complex microstructure in the welds that makes it more difficult for the dislocations to interact, the interaction distance in the weld zones has been assumed to be equal to 2 b. Since 2 b represents the core diameter of dislocations, it is the minimum possible value for the interaction distance. This should be compared with the corresponding value for parent metal, which is 2.5 b. The reduced interaction distance in the weld zones has two important consequences. First, the work hardening in the flow curves is reduced. Second, the strain in the creep tests gets larger. Both these effect are in full agreement with the observations.

The constitutive equations that have been set up are of fundamental nature. They are derived from basic physical principles. For parent metal it has been verified experimentally that the creep equations can be extrapolated to low stresses, which is of fundamental importance for any kind of long term prediction for the copper canisters. The equations for the weld zones have also been developed in such a way that they should be possible to use down to low stresses.

9 Conclusions

Slow strain rate tensile tests have been carried out for three types of specimens extracted from friction stir welds in Cu-OFP: weld zone, HAZ, and cross welds.

- A comparison is made to previously published flow curves for base metal. The base metal values for the yield strength are lower than in the weld microstructures. However, the work hardening in the weld zones is lower implying that some flow curves cross those of the parent metal.
- The elongation values for the weld microstructures measured at 1×10^{-4} and 3×10^{-6} 1/s show that the ductility is well above 20 %.
- A variation in yield strength of up to 25 MPa is observed for the weld zones. No such variation is found for the parent metal.
- The flow curves for the weld zones can be described by a similar model as for parent metal. The main difference is that the dislocation interaction distance is smaller during recovery for the weld zones.
- The same assumption concerning the dislocation interaction distance is made in the creep model. The difference between annealed and as delivered condition has been taken into account. In this way the creep model can represent creep strain versus time curves for weld zones.
- The numerical integration of the creep equations is nontrivial. Three different procedures for handling the numerical integration are presented giving similar results.

10 Acknowledgements

The authors wish to thank the Swedish Nuclear Fuel Waste Management Company (SKB) for financing this study and supplying test materials. Valuable help from Sören Claesson, SKB, is acknowledged. The authors are also grateful to Christina Lilja and Matts Björck, SKB for many useful comments and suggestions.

References

SKB's (Svensk Kärnbränslehantering AB) publications can be found at www.skb.com/publications.

ASM, 1991. ASM Handbook, Volume 2: Properties and selection: nonferrous alloys and special-purpose materials. Materials Park, OH: ASM International.

Andersson H, Seitisleam F, Sandström R, 1999. Influence of phosphorous and sulphur as well as grain size on creep in pure copper. SKB TR-99-39, Svensk Kärnbränslehantering AB.

Andersson H C M, Seitisleam F, Sandström R, 2007. Creep testing and creep loading experiments on friction stir welds in copper at 75 °C. SKB TR-07-08, Svensk Kärnbränslehantering AB.

Andersson-Östling H C M, Sandström R, 2009. Survey of creep properties of copper intended for nuclear waste disposal. SKB TR-09-32, Svensk Kärnbränslehantering AB.

Andersson-Östling H C M, Sandström R, 2011. Effect of loading rate on creep of phosphorous doped copper. SKB TR-11-09, Svensk Kärnbränslehantering AB.

Bergström Y, 1972. A dislocation model for the strain-ageing behaviour of steel. Materials Science and Engineering 9, 101–110.

Dieter G E, 1986. Mechanical metallurgy. 3rd ed. New York: McGraw-Hill.

Friedel J, 1964. Dislocations. Reading, MA: Addison-Wesley.

Hirth J P, Lothe J, 1968. Theory of dislocations. New York: McGraw-Hill.

Holdsworth S R, Askins M, Baker A, Gariboldi E, Holmstrom S, Klenk A, Ringel M, Merckling G, Sandström R, Schwienheer M, Spigarelli S, 2008. Factors influencing creep model equation selection. International Journal of Pressure Vessels and Piping 85, 80–88.

Horiuchi R, Otsuka M, 1973. Mechanism of high temperature creep of aluminum–magnesium solid solution alloys. Transactions of the Japan Institute of Metals 13, 284–293.

Jin L-Z, Sandström R, 2008. Creep of copper canisters in power-law breakdown. Computational Materials Science 43, 403–416.

Jin L-Z, Sandström R, 2009a. Non-stationary creep simulation with a modified Armstrong–Frederick relation applied to copper canisters. Computational Materials Science 46, 339–346.

Jin L-Z, Sandström R, 2009b. Modified Armstrong–Frederick relation for handling back stresses in FEM computations. In Shibli I A, Holdsworth S R (eds) Creep & fracture in high temperature components – design & life assessment issues: 2nd ECCC Creep Conference, Zürich, Switzerland, 21–23 April 2009. DEStech Publications, 836–847.

Jin L-Z, Sandström R, 2013. Influences of load variations on the plastic deformation in friction stir welds and contour slits in copper canisters. SKB TR-13-25, Svensk Kärnbränslehantering AB.

Kocks U F, Argon A S, Ashby M F, 1975. Thermodynamics and kinetics of slip. Oxford: Pergamon. (Progress in materials science 19.)

Korzhavyi P A, Sandström R, 2015. First-principles evaluation of the effect of alloying elements on the lattice parameter of a 23Cr25NiWCuCo austenitic stainless steel to model solid solution hardening contribution to the creep strength. Materials Science and Engineering: A 626, 213–219.

Ledbetter H M, Naimon E R, 1974. Elastic properties of metals and alloys. II. Copper. Journal of Physical and Chemical Reference Data 3, 897–935.

Mecking H, Kocks U F, 1981. Kinetics of flow and strain-hardening. Acta Metallurgica 29, 1865–1875.

Neumann G, Tölle V, Tuijn C, 1999. Monovacancies and divacancies in copper: reanalysis of experimental data. Physica B: Condensed Matter 271, 21–27.

Odqvist F K G, 1966. Mathematical theory of creep and creep rupture. Oxford: Clarendon.

Orlová A, 1991. On the relation between dislocation structure and internal stress measured in pure metals and single phase alloys in high temperature creep. Acta Metallurgica et Materialia 39, 2805–2813.

Raiko H, Sandström R, Rydén H, Johansson M, 2010. Design analysis report for the canister. SKB TR-10-28, Svensk Kärnbränslehantering AB.

Roberts W, Bergström Y, 1973. The stress-strain behaviour of single crystals and polycrystals of face-centered cubic metals – a new dislocation treatment. Acta Metallurgica 21, 457–469.

Rosborg B, Werme L, 2008. The Swedish nuclear waste program and the long-term corrosion behaviour of copper. Journal of Nuclear Materials 379, 142–153.

Roters F, Raabe D, Gottstein G, 2000. Work hardening in heterogeneous alloys – a microstructural approach based on three internal state variables. Acta Materialia 48, 4181–4189.

Sandström R, 2012. Basic model for primary and secondary creep in copper. Acta Materialia 60, 314–322.

Sandström R, 2016a. Fundamental models for creep properties of steels and copper. Transactions of the Indian Institute of Metals 69, 197–202.

Sandström R, 2016b. Influence of phosphorus on the tensile stress strain curves in copper. Journal of Nuclear Materials 470, 290–296.

Sandström R, 2016c. The role of cell structure during creep of cold worked copper. Materials Science and Engineering: A 674, 318–327.

Sandström R, Hallgren J, 2012. The role of creep in stress strain curves for copper. Journal of Nuclear Materials 422, 51–57.

Sandström R, Andersson H C M, 2008a. Creep in phosphorus alloyed copper during power-law breakdown. Journal of Nuclear Materials 372, 76–88.

Sandström R, Andersson H C M, 2008b. The effect of phosphorus on creep in copper. Journal of Nuclear Materials 372, 66–75.

Sandström R, Hallgren J, Burman G, 2009. Stress strain flow curves for Cu-OFP. SKB R-09-14, Svensk Kärnbränslehantering AB.

Sandström R, Östling H, Jin L-Z, 2013. Modelling of creep in friction stir welded copper. Materials Research Innovations 17, 350–354.

Wang R, Wang S, Wu X, 2011. Edge dislocation core structures in FCC metals determined from *ab initio* calculations combined with the improved Peierls–Nabarro equation. Physica Scripta 83. doi:10.1088/0031-8949/83/04/045604

Wu R, Jin L-Z, Sandström R, 2010. Influence of multiaxial stresses on creep properties of phosphorus alloyed oxygen free copper. In ASME 2009 Pressure Vessels and Piping Conference (PVP 2009), Prague, 26–30 July 2009. American Society of Mechanical Engineers, Volume 6: Materials and Fabrication, Parts A and B, 1525–1532.

Wu R, Pettersson N, Martinsson Å, Sandström R, 2014. Cell structure in cold worked and creep deformed phosphorus alloyed copper. Materials Characterization 90, 21–30.

Yao X, Sandström R, 2000. Study of creep behaviour in P-doped copper with slow strain rate tensile tests. SKB TR-00-09, Svensk Kärnbränslehantering AB.

Appendix A

Table A-1a. Values for K (and σ_{stat}) (MPa) cf. Eq (4-15) for ω = 14.67, parent metal.

Temp. °C	$\dot{\varepsilon}$ 1/s	1×10^{-2}	1×10^{-3}	1×10^{-4}	1×10^{-5}	1×10^{-6}	1×10^{-7}	1×10^{-8}	1×10^{-9}	1×10^{-10}
0		227.8	223.7	219.6	215.4	211.1	206.7	202.2	197.6	192.9
25		220.8	216.3	211.7	207.0	202.1	197.2	192.1	186.8	181.5
50		213.9	208.8	203.7	198.4	193.0	187.4	181.7	175.8	169.6
75		206.8	201.2	195.6	189.7	183.7	177.4	171.0	164.3	157.3
100		199.6	193.5	187.3	180.8	174.1	167.2	159.9	152.3	144.4
125		193.0	186.4	179.5	172.4	165.0	157.2	149.1	140.5	131.4
150		186.9	179.6	172.1	164.3	156.0	147.4	138.3	128.5	118.1
175		180.6	172.7	164.5	155.9	146.8	137.1	126.9	115.8	103.8
200		174.6	166.0	157.0	147.5	137.5	126.7	115.1	102.4	88.3

Table A-1b. Values for K (and σ_{stat}) (MPa), cf. Eq (4-15) for ω = 11.73, weld zones.

Temp. °C	$\dot{\varepsilon}$ 1/s	1×10^{-2}	1×10^{-3}	1×10^{-4}	1×10^{-5}	1×10^{-6}	1×10^{-7}	1×10^{-8}	1×10^{-9}	1×10^{-10}
0		219.1	215.0	210.9	206.6	202.3	197.9	193.4	188.8	184.1
25		213.2	208.7	204.1	199.4	194.5	189.6	184.5	179.2	173.8
50		207.4	202.3	197.2	191.9	186.5	180.9	175.2	169.2	163.1
75		201.4	195.8	190.2	184.3	178.2	172.0	165.5	158.8	151.8
100		195.3	189.2	183.0	176.5	169.8	162.8	155.5	147.9	140.0
125		189.4	182.8	175.9	168.7	161.3	153.5	145.4	136.8	127.7
150		183.7	176.5	168.9	161.0	152.8	144.1	134.9	125.2	114.7
175		177.9	170.0	161.7	153.0	143.9	134.2	123.9	112.8	100.7
200		172.1	163.5	154.4	144.9	134.8	124.0	112.3	99.5	85.4

Table A-2a. Values for c_L for ω = 14.67 (parent metal), cf. Eq (4-15).

Temp. °C	$\dot{\varepsilon}$ 1/s	1×10^{-2}	1×10^{-3}	1×10^{-4}	1×10^{-5}	1×10^{-6}	1×10^{-7}	1×10^{-8}	1×10^{-9}	1×10^{-10}
0		24.5	25.0	25.4	25.9	26.5	27.0	27.6	28.3	29.0
25		24.8	25.4	25.9	26.5	27.1	27.8	28.6	29.4	30.2
50		25.2	25.8	26.5	27.2	27.9	28.7	29.7	30.7	31.8
75		25.6	26.3	27.1	27.9	28.8	29.8	30.9	32.2	33.6
100		26.0	26.8	27.7	28.7	29.8	31.1	32.5	34.1	36.0
125		26.4	27.3	28.4	29.6	30.9	32.4	34.2	36.3	38.8
150		26.7	27.8	29.0	30.4	32.0	33.9	36.1	38.9	42.3
175		27.1	28.4	29.8	31.4	33.4	35.7	38.6	42.3	47.2
200		27.5	28.9	30.6	32.5	34.9	37.9	41.7	46.9	54.4

Table A-2b. Values for c_L for ω = 11.73 (weld zones), cf. Eq (4-15).

Temp. °C	$\dot{\varepsilon}$ 1/s	1×10^{-2}	1×10^{-3}	1×10^{-4}	1×10^{-5}	1×10^{-6}	1×10^{-7}	1×10^{-8}	1×10^{-9}	1×10^{-10}
0		31.9	32.5	33.1	33.8	34.5	35.3	36.1	37.0	37.9
25		32.2	32.9	33.6	34.4	35.3	36.2	37.2	38.3	39.5
50		32.5	33.3	34.2	35.1	36.1	37.2	38.5	39.8	41.3
75		32.9	33.8	34.8	35.9	37.1	38.5	40.0	41.7	43.6
100		33.3	34.3	35.5	36.8	38.3	39.9	41.8	43.9	46.4
125		33.6	34.9	36.2	37.8	39.5	41.5	43.8	46.6	49.9
150		34.0	35.4	37.0	38.8	40.9	43.4	46.3	49.9	54.5
175		34.5	36.1	37.9	40.0	42.6	45.7	49.5	54.3	60.9
200		34.9	36.7	38.9	41.5	44.6	48.5	53.5	60.4	70.4

Table A-3. Values for the creep exponent n_N for $\sigma = \sigma_{stat}$ from Eq (6-2).

Temp. °C	$\dot{\varepsilon}$ 1/s	1×10^{-2}	1×10^{-3}	1×10^{-4}	1×10^{-5}	1×10^{-6}	1×10^{-7}	1×10^{-8}	1×10^{-9}	1×10^{-10}
0		121.3	116.7	112.2	107.8	103.3	98.9	94.5	90.1	85.7
25		106.4	101.9	97.4	93.0	88.6	84.2	79.8	75.4	71.0
50		93.8	89.4	85.0	80.6	76.2	71.8	67.4	63.1	58.8
75		83.1	78.7	74.4	70.0	65.6	61.3	56.9	52.6	48.3
100		73.9	69.5	65.2	60.8	56.5	52.2	47.9	43.7	39.4
125		65.9	61.5	57.2	52.9	48.6	44.3	40.1	35.9	31.8
150		58.8	54.5	50.2	45.9	41.7	37.5	33.3	29.2	25.1
175		52.6	48.3	44.0	39.8	35.6	31.5	27.4	23.4	19.5
200		47.0	42.8	38.6	34.4	30.2	26.2	22.2	18.3	14.6

Table A-4a. Values for σ_y/σ_{yref} for parent metal according to Eq (4-19).

Temp. °C	$\dot{\varepsilon}$ 1/s	1×10^{-2}	1×10^{-3}	1×10^{-4}	1×10^{-5}	1×10^{-6}	1×10^{-7}	1×10^{-8}	1×10^{-9}	1×10^{-10}
0		1.051	1.033	1.014	0.994	0.974	0.951	0.928	0.903	0.876
25		1.036	1.018	0.996	0.974	0.950	0.924	0.896	0.866	0.834
50		1.025	1.003	0.979	0.953	0.925	0.895	0.862	0.827	0.788
75		1.013	0.988	0.961	0.932	0.900	0.864	0.826	0.783	0.736
100		1.001	0.973	0.943	0.910	0.873	0.832	0.786	0.735	0.678
125		0.990	0.959	0.925	0.888	0.845	0.798	0.744	0.683	0.613
150		0.979	0.945	0.908	0.865	0.816	0.761	0.697	0.624	0.539
175		0.969	0.932	0.890	0.842	0.786	0.721	0.645	0.556	0.453
200		0.959	0.919	0.872	0.817	0.753	0.677	0.586	0.479	0.356

Table A-4b. Values for σ_y/σ_{yref} for weld zones according to Eq (4-19).

Temp. °C	$\dot{\varepsilon}$ 1/s	1×10^{-2}	1×10^{-3}	1×10^{-4}	1×10^{-5}	1×10^{-6}	1×10^{-7}	1×10^{-8}	1×10^{-9}	1×10^{-10}
0		1.063	1.034	1.014	0.994	0.972	0.949	0.924	0.898	0.870
25		1.039	1.018	0.996	0.973	0.948	0.921	0.892	0.861	0.828
50		1.026	1.003	0.979	0.952	0.923	0.892	0.858	0.821	0.781
75		1.014	0.989	0.961	0.931	0.898	0.862	0.822	0.778	0.730
100		1.002	0.974	0.943	0.909	0.871	0.830	0.783	0.731	0.672
125		0.991	0.960	0.925	0.887	0.844	0.795	0.740	0.678	0.607
150		0.980	0.946	0.908	0.864	0.815	0.758	0.694	0.619	0.533
175		0.970	0.933	0.890	0.841	0.784	0.718	0.641	0.551	0.447
200		0.960	0.919	0.872	0.817	0.752	0.674	0.582	0.474	0.349